NAVAL POSTGRADUATE SCHOOL
Monterey, California

THESIS

AN AUTONOMOUS CIRCUIT FOR THE MEASUREMENT OF PHOTOVOLTAIC DEVICES PARAMETERS
by

Robert Kendall Callaway

September 1986

Thesis Advisor: Sherif Michael

SECURITY CLASSIFICATION OF THIS PAGE

REPORT DOCUMENTATION PAGE

1a REPORT SECURITY CLASSIFICATION UNCLASSIFIED	1b RESTRICTIVE MARKINGS
2a SECURITY CLASSIFICATION AUTHORITY	3 DISTRIBUTION / AVAILABILITY OF REPORT Approved for public release; distribution is unlimited
2b DECLASSIFICATION / DOWNGRADING SCHEDULE	
4 PERFORMING ORGANIZATION REPORT NUMBER(S)	5 MONITORING ORGANIZATION REPORT NUMBER(S)
6a NAME OF PERFORMING ORGANIZATION Naval Postgraduate School 6b OFFICE SYMBOL (If applicable) 62	7a NAME OF MONITORING ORGANIZATION Naval Postgraduate School
6c ADDRESS (City, State, and ZIP Code) Monterey, California 93943-5000	7b ADDRESS (City, State, and ZIP Code) Monterey, California 93943-5000
8a NAME OF FUNDING / SPONSORING ORGANIZATION 8b OFFICE SYMBOL (If applicable)	9 PROCUREMENT INSTRUMENT IDENTIFICATION NUMBER
8c ADDRESS (City, State, and ZIP Code)	10 SOURCE OF FUNDING NUMBERS PROGRAM ELEMENT NO / PROJECT NO / TASK NO / WORK UNIT ACCESSION NO

11 TITLE (Include Security Classification)
AN AUTONOMOUS CIRCUIT FOR MEASUREMENT OF PHOTOVOLTAIC DEVICES PARAMETERS

12 PERSONAL AUTHOR(S)
Callaway , Robert K

13a TYPE OF REPORT	13b TIME COVERED	14 DATE OF REPORT (Year, Month, Day)	15 PAGE COUNT
Master's Thesis	FROM _____ TO _____	1986 September	86

16 SUPPLEMENTARY NOTATION

17 COSATI CODES			18 SUBJECT TERMS (Continue on reverse if necessary and identify by block number)
FIELD	GROUP	SUB-GROUP	Photovoltaic Devices; Solar Cell; Space Based; Test Circuit

19 ABSTRACT (Continue on reverse if necessary and identify by block number)

In this research a novel autonomous test system is presented. The system is a self contained microprocessor based experiment, which was developed to compare and test different state-of-the-art Gallium Arsenide and Silicon solar cells. The result will help evaluate radiation hardness properties of both types of solar cells. The system can also be used to study the annealing process as well as shadowing effects in space array systems. Stringent requirements were considered in designing the system for durable operation in a space environment.

20 DISTRIBUTION / AVAILABILITY OF ABSTRACT	21 ABSTRACT SECURITY CLASSIFICATION
☒ UNCLASSIFIED/UNLIMITED ☒ SAME AS RPT ☐ DTIC USERS	UNCLASSIFIED
22a NAME OF RESPONSIBLE INDIVIDUAL Prof Sheriff Michael	22b TELEPHONE (Include Area Code) (408)646-2252 22c OFFICE SYMBOL 62Mi

DD FORM 1473, 84 MAR 83 APR edition may be used until exhausted
All other editions are obsolete

SECURITY CLASSIFICATION OF THIS PAGE

Approved for public release; distribution is unlimited.

An Autonomous Circuit for the Measurement of Photovoltaic Devices Parameters

by

Robert Kendall Callaway
Lieutenant, United States Navy
B.A., California State University, Chico, 1978

Submitted in partial fulfillment of the
requirements for the degree of

MASTER OF SCIENCE IN ELECTRICAL ENGINEERING

from the

NAVAL POSTGRADUATE SCHOOL
September 1986

ABSTRACT

In this research a novel autonomous test system is presented. The system is a self contained microprocessor based experiment, which was developed to compare and test different state-of-the-art Gallium Arsenide and Silicon solar cells. The result will help evaluate radiation hardness properties of both types of solar cells. The system can also be used to study the annealing process as well as shadowing effects in space array systems. Stringent requirements were considered in designing the system for durable operation in a space environment.

TABLE OF CONTENTS

LIST OF FIGURES..... 6

TABLE OF SYMBOLS..... 8

I. INTRODUCTION..... 12

A. FORWARD: PHOTOVOLTAIC TECHNOLOGY AND SPACE... 12

B. PROPOSED RESEARCH..... 14

C. OVERVIEW OF THESIS..... 17

II. PHOTOVOLTAIC EFFECT..... 18

A. SEMICONDUCTOR THEORY..... 18

B. CARRIER TRANSPORT..... 23

C. DC MODEL THEORY..... 25

D. IMPROVEMENTS IN SOLAR CELLS..... 35

E. DAMAGE TO SOLAR CELLS..... 39

1. Radiation Damage Theory..... 40

a. Ionization..... 41

b. Atomic Displacement..... 41

2. Silicon Solar Cell Damage..... 42

3. Concept of Damage Equivalence..... 45

4. Irradiation of Silicon Solar Cells..... 46

5. Solar Cell Degradation, Electrons..... 48

6. Solar Cell Degradation, Protons..... 50

7. Junction Damage (Low Energy Protons).... 52

8. Radiation Damage Annealing..... 53

III. PHOTOVOLTAIC TESTING..... 54

A. HISTORICAL BACKGROUND..... 54

B. SINGLE CELL MEASUREMENTS..... 56

C. PRESENT METHODS OF TESTING PHOTOVOLTAIC DEVICES..... 57

D. METHODS OF TESTING CELLS IN SPACE..... 60

1. LIPS-II Solar Cell Experiment..... 60

2. NTS-2 Satellite..... 63

3. Solar Cell Calibration Experiment (SCCE)..... 65

E. SOLAR SIMULATOR AT NPS..... 65

IV. NOVEL PHOTOVOLTAIC TESTING SYSTEM..... 67

A. PROPOSED CIRCUIT..... 67

1. Design Requirements..... 68

2. Alternative Circuits Considered..... 69

B. NOVEL CIRCUIT DESIGN..... 70

1. Circuit Development..... 71

2. Controlling the Test Circuit Using a Microprocessor..... 73

V. CONCLUSIONS..... 77

A. RESULTS..... 77

B. RECOMMENDATIONS..... 77

LIST OF REFERENCES..... 82

INITIAL DISTRIBUTION LIST..... 84

LIST OF FIGURES

1.1 Military Space Power Requirements 1980 - 2000.... 13

1.2 Maximum Single-Spacecraft Power by Year..... 14

1.3 Solar Cell Test System Diagram..... 15

1.4 GAS Satellite Launching from Shuttle..... 16

2.1 Cross Section of Solar Cell..... 26

2.2 Hypothetical Concentrations of Holes and Electrons in a Solar Cell..... 27

2.3 Actual Concentration of Holes and Electrons..... 29

2.4 Light Incident on Cell Creates Electron-Hole Pairs..... 30

2.5 Charge Density in Depletion Region..... 31

2.6 Electrostatic Potential in Solar Cells..... 31

2.7 Solar Cell Equivalent Circuit..... 33

2.8 Hole and Electron Current Densities..... 34

2.9 Spectral Response of Several Semiconductor Materials..... 35

2.10 Change in Spectral Response Due to Cell Thickness..... 36

2.11 Modified Solar Cell Equivalent Circuit..... 37

2.12 Effect of Shunt Resistance on I-V Curve..... 38

2.13 Effect of Series Resistance on I-V Curve..... 39

2.14 Example I-V Curve..... 42

2.15 Variation in I_{SC} for Various Radiations..... 44

2.16 Spectral Response of a Silicon Cell; Nonirradiated..... 47

2.17 Spectral Response of a Silicon Cell; Irradiated with 1 MeV Electrons..... 48

2.18 Atom Displacements as a Function of Depth (3 MeV Proton in Silicon)..... 49

2.19 Relative Damage Coefficients for Proton-Irradiated Silicon Cells..... 51

3.1 Measuring Circuit for Method (1)..... 58

3.2 LIPS-II, Living Plume Shield..... 60

3.3 LIPS Maximum Power vs Days from Launch..... 62

3.4 NTS-2 Satellite..... 63

3.5 Typical NTS-2 I-V Curve..... 64

4.1 Novel Circuit Design..... 71

4.2 Solar Cell Subcircuit..... 72

4.3 System Layout..... 76

5.1a Comparison Data, Silicon..... 78

5.1b Comparison Data, Silicon..... 79

5.2 Comparison Data, Gallium Arsenide..... 80

TABLE OF SYMBOLS

A	Curve Fitting Constant
ADC	Analog to Digital Converter
AM0	Air-Mass-Zero; Sunlight Concentration at Earth's Orbit
ATS-1	Solar Cell Test Satellite Launched in 1966
BJT	Bipolar Junction Transistor
C	Decrease in I_{sc} per Decade in Radiation Fluence in the Logarithmic Region
CMOS	Complementary Metal-Oxide Semiconductor
DAC	Digital to Analog Converter
DC	Direct Current
D_p	Hole Diffusion Constant (cm^2/sec)
dn/dx	Gradient of Electron Concentration
dp/dx	Gradient of Hole Concentration
E	Electric Field (V/cm)
E_G	Bandgap Energy (1.11 eV in Si at 300^o K)
eV	Electron Volts
GaAs	Gallium Arsenide
g_{ext}	Excitation Rate per Unit Volume due to an External Cause,
g_{th}	Thermal Generation Rate,
h_{fe}	Common Emitter Transistor Current Gain
I	Current in Load
I_C	Current in the Collector
I_E	Current in the Emitter

I_L	Photovoltaic Current Across the Junction
I_o	Reverse Saturation Current in Diode
I_{RE}	Transistor Emitter Resistance Current
I_{sc}	Short Circuit Current, Maximum Current the Cell can Generate when it's Two Terminals are Short Circuited
I-V	Current versus Voltage Curve
J	Total Current Density
J_D	Current Across Simulated Diode
J_{jn}	Flow of Electrons back through the Junction
J_L	Light Generated Current
J_n	Electron Current Density (amps/cm^2)
J_{nn}	Electron Drift Current
J_{np}	Electron Diffusion Current (injected minority carriers)
J_o	Diode Saturation Current
J_p	Hole Current Density (amps/cm^2)
J_{ph}	Photon Excited Current
J_{pn}	Hole Diffusion Current (injected minority carriers)
J_{pp}	Hole Drift Current
k	Bolztman Constant (8.6171 x 10^{-5} eV/k)
K	Temperature in Kelvin
LIPS	Living Plume Shield, Solar Cell Satellite-II
L_n	Diffusion Length in n-material
L_p	Diffusion Length in p-material
MeV	10^6 Electron Volts

n_i	Intrinsic Carrier Concentration (cm^{-3}) Electrons
n_o	Equilibrium Concentration of Conduction Electrons (cm^{-3})
n_{po}	Thermal Equilibrium Concentration of Electrons in p-type Material
N_t	Density of the Recombination Centers
NTS-2	Navigation Technology Satellite-Two
n-	Negatively Doped Semiconductor Material
n(t)	Total Instantaneous Electron Concentrations in n-material
n'(t)	Instantaneous Excess Electron Concentrations
p	Hole Concentration (cm^{-3})
p_i	Intrinsic Carrier Concentration (cm^{-3}), Holes
P_{mp}	Maximum Power Point, Power at the Knee of the I-V Curve
p_n	Concentration of Holes in n-type Material
p_{no}	Thermal Equilibrium Concentration of Holes in n-type Material
p_o	Equilibrium Concentration of Holes (cm^{-3})
p(t)	Total Instantaneous Electron Concentrations in n-material
p_n	(x)Hole Concentration at a Distance (x) from the Junction
p-	Positively Doped Semiconductor Material
p'(t)	Instantaneous Excess Hole Concentrations
$p'_n(t)$	Instantaneous Excess Hole Concentrations in n-material

q	Hole Charge (coulomb)
r	Total Recombination Rate
R_E	Resistor in the Emitter Leg of Transistor
R_{sh}	Shunt Resistance Across the Junction
R_{sr}	Series Resistance
SCCE	Solar Cell Calibration Experiment
SDIO	Strategic Defense Initiative Office
Si	Silicon
T	Temperature (K)
u	Net Rate of Recombination
V_o	Potential Barrier in Solar Cell
V_{oc}	Open Circuit Voltage, Voltage Across the Cells Terminals when Circuit is not Loaded
V_{th}	Thermal Velocity of an Excess Carrier (approximately 10^7 cm/sec for Silicon)
σ_p	Cross Section for Capture of a Hole by a Recombination Center
ρ	Resistivity of the Semiconductor Material
τ_n	Lifetime of a Electron
τ_p	Lifetime of a Hole
μ_p	Hole Mobility (cm^2)
ϕ_c	Solar Cell Critical Radiation Fluence
ϕ_x	Radiation Fluence at which I_{sc} Starts to Change to a Linear Function of the Logarithm of the Fluence

I. INTRODUCTION

A. FORWARD: PHOTOVOLTAIC TECHNOLOGY AND SPACE

In the last three decades, photovoltaic technology has made impressive strides and has been the backbone of the Space Program (Figure 1.1) [Ref. 1]. Solar cells have filled the skies from deep space planetary exploration to most imaginable orbits about earth. Performance has steadily improved, durability refined and cost held stable. The vast majority of present day satellites are powered by solar cells. Both military and commercial planners (NASA) are forecasting a continuation of high capacity space systems (Figure 1.2). Supporting that need, but separate from it is the opportunity to reduce significantly the mass of the power system of the orbiting spacecraft. With power system mass currently equalling payload mass, obvious opportunities exist to provide more power at less weight for commercial purpose. [Ref. 1]

With the development of the Global Positioning Satellite system (GPS) in synchronous orbits and present day geosynchronous orbit operation, there is a significant need to boost the radiation tolerance of solar cells. Such increased tolerance not only raises end-of-life power, which reduces the size and mass of the array, it also flattens the change

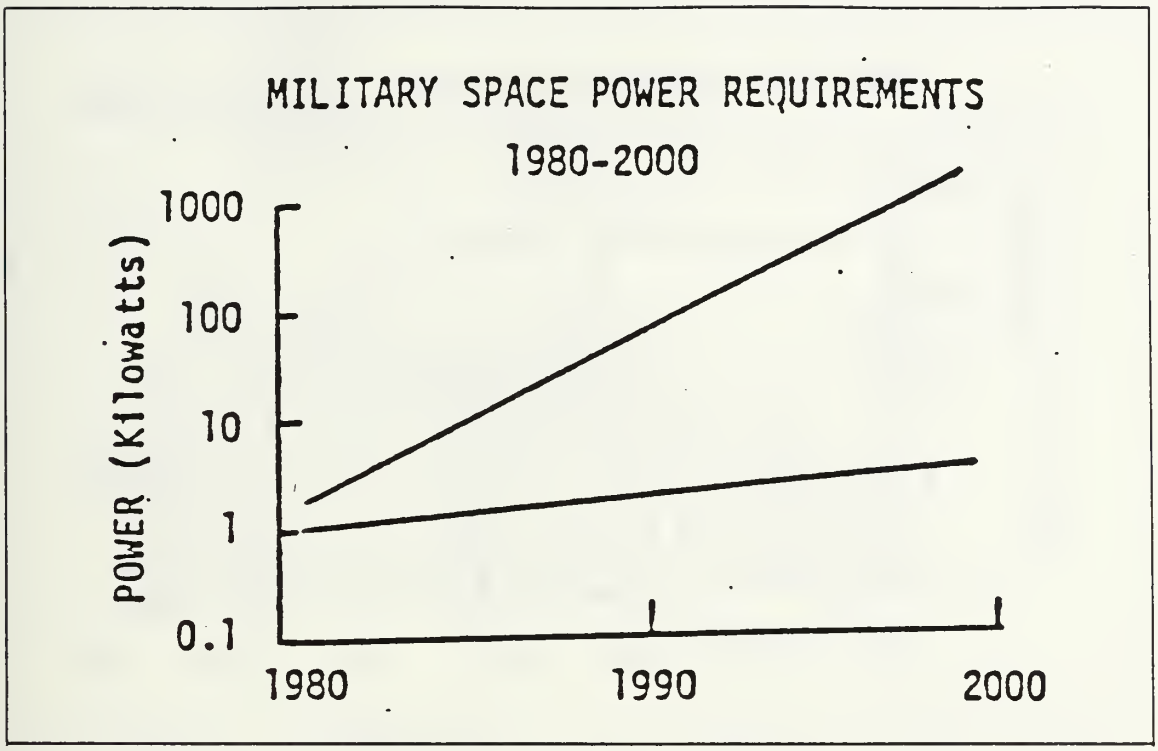

Figure 1.1 Military Space Power Requirements 1980 - 2000

of power with time which can lead to power system simplification. Increased radiation resistance will also open the door to the radiation intensive orbits providing additional benefit and flexibility to mission planners. Additionally, planetary needs continue to be important. [Ref. 2]

Using Gallium Arsenide (GaAs) solar cells was a major step toward achieving this goal. Moreover GaAs [Refs. 3, 4] cells were found to be more radiation hardened than state-of-the-art silicon solar cells. Since current testing facilities do not fully simulate the conditions of space, testing of advanced solar cells must be accomplished in a space environment.

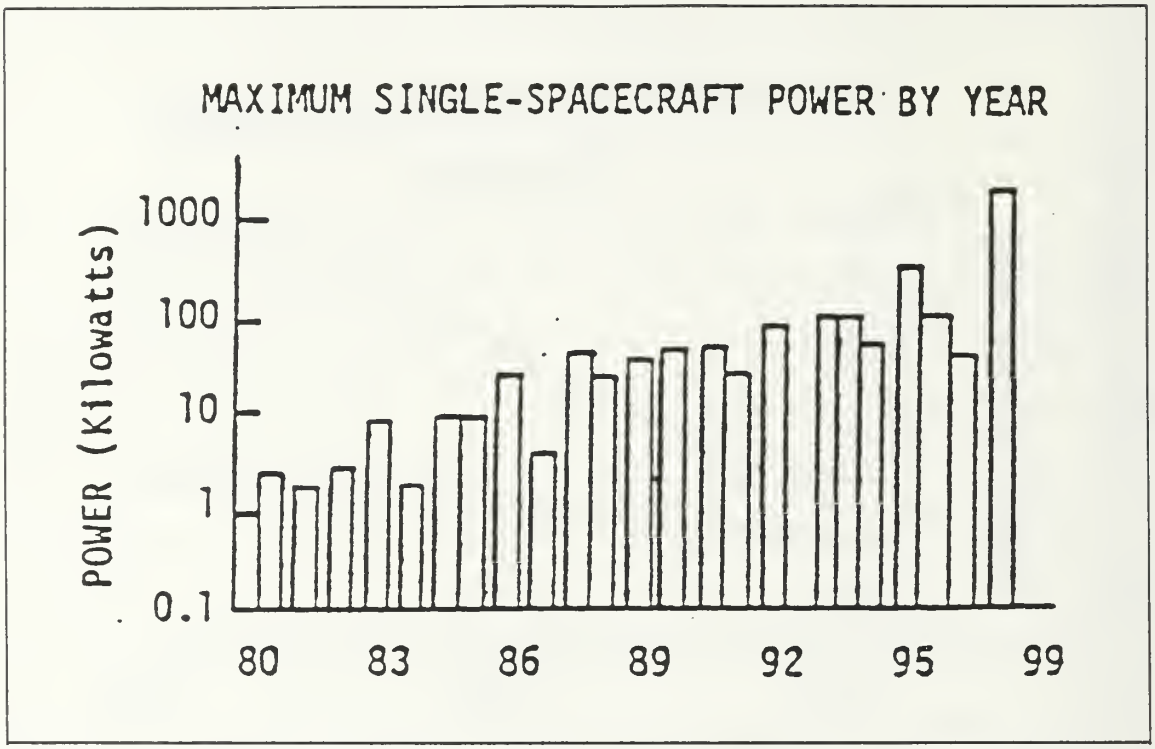

Figure 1.2 Maximum Single-Spacecraft Power by Year

B. PROPOSED RESEARCH

In this thesis, a self contained experiment has been developed to compare and test different state-of-the-art solar cells (Figure 1.3). The experiment was originally designed for a Navy TRANSIT satellite but the design was later generalized to fit any platform because of its low power consumption advantage.

A General Purpose Satellite is being developed by the Naval Postgraduate School Space Research Group for USAF/SDIO defense and Experimenter missions [Ref. 5]. It will provide full satellite support services for small payloads of up to 70 pounds, and can be launched from the Shuttle into circular

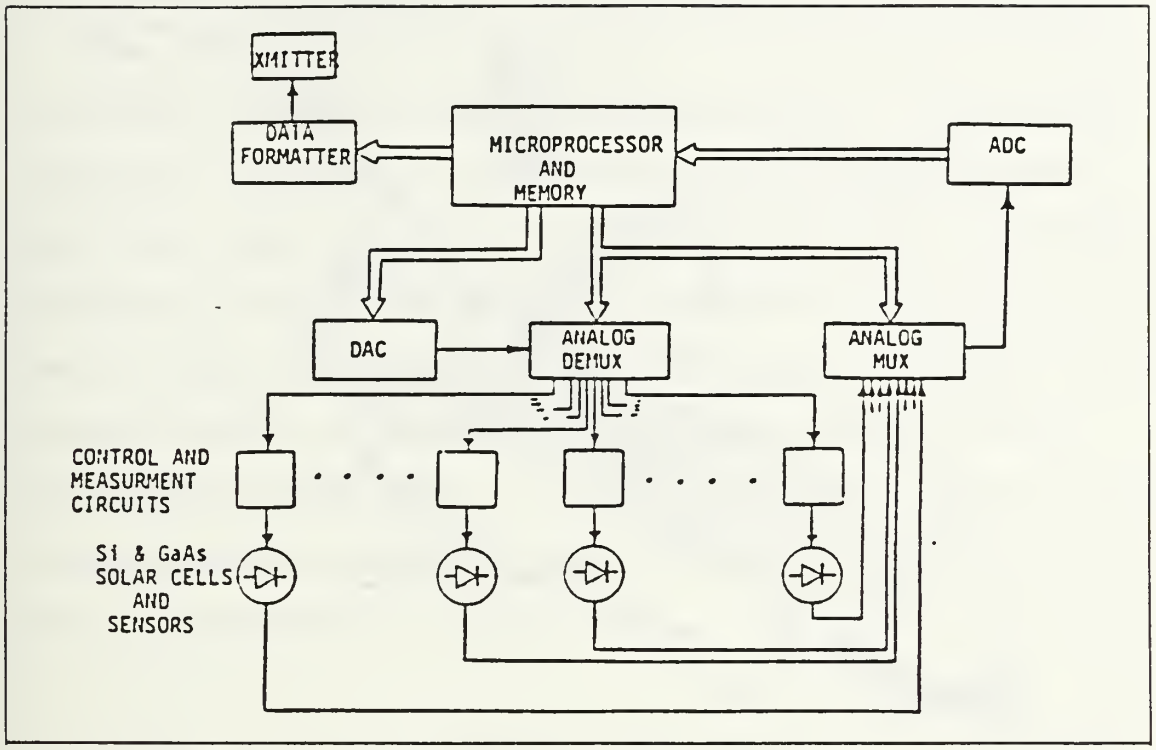

Figure 1.3 Solar Cell Test System Diagram

orbits with a radius of 2000 km, or elliptical orbits with an apogee of 12000 km. Using a second generation Get-Away-Special (GAS) Satellite ejection concept, or an optional deployment from expandable launch vehicles, the satellite will enable government and industry to access the low earth orbits for less than $600,000 per flight unit (Figure 1.4). [Ref. 5]

The solar cell project is now being redesigned as a "piggy-back" experiment on an ongoing research project to be launched into the Van Allen radiation belt region. The major objective will be studying the long term degradation caused by radiation and temperature on individual solar cells.

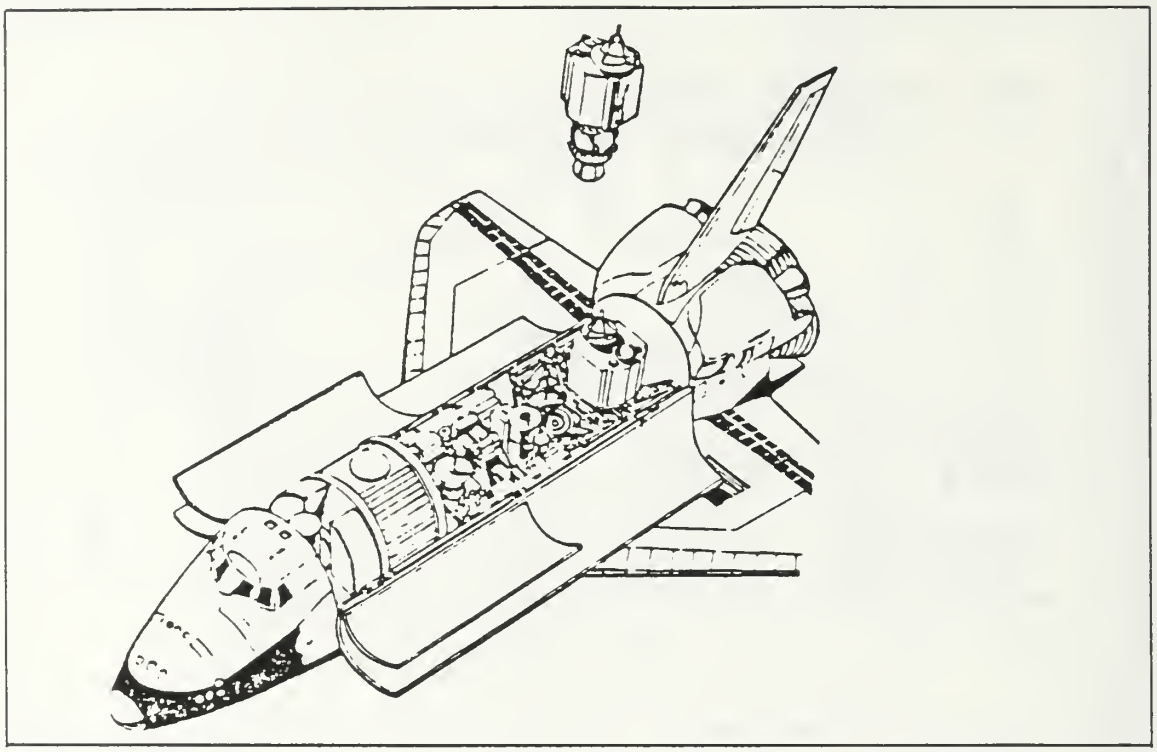

Figure 1.4 GAS Satellite Launching from Shuttle.

In this thesis the development of a self-contained microprocessor system (Figure 1.3) is presented. The proposed system is designed according to the following guidelines:

(1) To be able to measure the I-V characteristics of individual solar cells. A novel circuit is developed that uses a microprocessor controlled Digital to Analog Converter (DAC) to obtain discrete points along the I-V curve of the test cell.

(2) The multiplexed data acquired from each cell, as well as onboard sensors, will be digitized and stored in memory.

(3) The integrated system has been designed to use the satellite's power system.

C. OVERVIEW OF THESIS

The organization of the thesis is as follows. Chapter 2 contains a review of the photovoltaic effect. This review consists of looking at semiconductor and DC model theory, solar cell improvement and damage to solar cells. Chapter 3 presents a overview of photovoltaic testing from the earliest tests to present day testing in space and at the Naval Postgraduate School. In Chapter 4 the requirements and the development of the novel circuit is discussed. The results of the research as well as recommendations for future projects is presented in Chapter 5.

II. PHOTOVOLTAIC EFFECT

A. SEMICONDUCTOR THEORY

A family of materials known as semiconductors have electrical and physical characteristics that fall between metals and dielectrics. Semiconductors have four electrons in their outermost (valence) shell. Pure silicon crystals have four valence electrons which are bonded (shared) with four adjoining atoms, such that each atom will have eight electrons shared in its outermost shell. This type of bonding formed by shared electrons is called covalent bonding. The potential required to remove any of these four valence electrons is lower than that required for any other electrons.

Semiconductors have a unique characteristic that allows bipolar conduction. This is where charge transport can occur by conduction band electrons or through empty energy states in the valence band which behave electrically like positively charged electrons. These are known as holes. The thermal environment determines equilibrium concentrations of conduction electrons and holes in silicon as shown in the following equation. [Ref. 6]

$$n_o p_o = n_i^2 = 3.62 \times 10^{31}\, T^3 \exp(-E_G/kT), \quad (2.1)$$
$$= 2.2 \times 10^{20}\ cm^{-6}, \text{ for } T = 300\ K$$

where n_o = the equilibrium concentration of conduction electrons (cm^{-3})

p_o = the equilibrium concentration of holes (cm^{-3})

n_i = intrinsic carrier concentration (cm^{-3})

E_G = bandgap energy (1.11 eV in Si at 300°K)

T = temperature (K)

k = Bolztman constant (8.6171×10^{-5} eV/K)

For a semiconductor that is highly purified, thermal excitation across the band gap, (from the valence band to the conduction band) is the principal source of charge carriers, and the concentration of conduction electrons will equal the concentration of holes. In the state in which the electrical properties of the material is not modified by impurities, the semiconductor material is called intrinsic. At room temperature the electron and hole concentrations, n_i, in intrinsic silicon are equal to 1.5×10^{10} cm^{-3}.

If elements from Group III and V of the periodic table appear in a solid solution of silicon, they can be thermally ionized. If a Group V element such as phosphorus or arsenic is introduced into silicon the resulting ionization will introduce an electron in the conduction band and a positively charged donor atom in the silicon lattice. Conversely a Group III element, such as boron, will cause a hole to be present in the valence band and a negatively charged acceptor ion. The energies required to activate the donor and acceptor atoms in silicon are approximately 0.05 eV. Since equilibrium will be reached at temperatures near 300° K, commonly

used impurities from Groups III and V can be considered completely ionized at room temperatures.

Extrinsic semiconductor material is formed when impurities are added to intrinsic materials by a process known as doping. An n-type (negative type) extrinsic semiconductor is one that has an equilibrium concentration of conduction electrons that exceeds the intrinsic carrier concentration. Conversely a p-type material is when the equilibrium concentration of holes exceeds the intrinsic carrier concentration of the semiconductor. Equation 2.1 which can also describe the product of the equilibrium conduction electron and hole concentrations in extrinsic semiconductors will remain constant. A boron doped, p-type, extrinsic silicon cell that has a hole concentration of 1.4×10^{15} cm^{-3} must have a conduction electron concentration of 1.6×10^{5} cm^{-3}. The holes are considered the majority carriers while the conduction electrons are described as the minority carriers.

An increase in the concentration of conduction electrons and holes above the values at thermal equilibrium can be introduced by absorption of electromagnetic radiation. Equations 2.2 and 2.3 describes the total instantaneous concentrations of carriers for p- and n-type materials during an excitation process. [Ref. 6]

$$p(t) = p_o + p'(t), \qquad (2.2)$$

$$n(t) = n_o + n'(t), \qquad (2.3)$$

where $p'(t)$ and $n'(t)$ are instantaneous excess electron and hole concentrations.

p_o = the equilibrium concentration of holes (cm^{-3})

n_o = the equilibrium concentration of conduction electrons (cm^{-3})

Optical injection of carriers or optical absorption is the process whereas the cell absorbs electromagnetic radiation. This is essential to the operation of a solar cell. During this process, an electron-hole pair is created for each photon of light absorbed with sufficient energy. Different solar cell materials have different characteristic energies at which electrons are freed (energy must be greater than the bandgap energy, [Ref. 6]). For silicon the bandgap energy is 1.2 eV, Gallium Arsenide is 1.4 eV. Photons with energy in this range will create electron-hole pairs upon absorption in such material (more details in section C). The following equation (2.4) define the densities of the excess electrons and holes in intrinsic silicon.

$$dp_i(t)/dt = dn_i(t)/dt = g_{ext} + g_{th} - r, \quad (2.4)$$

where g_{ext} = excitation rate per unit volume due to an external cause

g_{th} = thermal generation rate

r = total recombination rate

Equation 2.4 can be further refined by defining, u, as the net rate of recombination. This value is defined by the following equation:

$$u = r - g_{th}, \quad (2.5)$$

Therefore equations 2.4 can be rewritten as:

$$dp_i(t)/dt = dn_i(t)/dt = g_{ext} - u, \quad (2.6)$$

The above equations are for intrinsic semiconductor.

On the other hand considering extrinsic materials at low injection levels ($p'(t) << n_o$) in n-type semiconductors a good approximation for, u,is:

$$u = (p_n - p_{no})/\tau_p = p'(t)/\tau_p, \quad (2.7)$$

where $p'(t)$ = defined as in equation 2.2,

τ_p = lifetime of a hole

p_n = concentration of holes in n-type material

p_{no} = thermal equilibrium concentration

Integration of equation 2.6, the time derivative of p(t), for the case of $g_{ext} = 0$, and the initial condition $p_n(0) = p_{no}$. The result will show that the lifetime is now seen to

be the decay time constant governing the recombination of excess holes in the n-material as, t, approaches zero. [Ref. 6]

$$p'_n(t) = p_n(0)e^{-t/\tau_p}, \quad (2.8)$$

An exact definition (as defined by Shockely) for the lifetime, τ_p, is given by the equation, (for holes):

$$\tau_p \propto (\sigma_p \, V_{th} \, N_t)^{-1}, \quad (2.9)$$

where σ_p = cross section for capture of a hole by a recombination center

V_{th} = thermal velocity of an excess carrier (approximately 10^7 cm/sec for silicon)

N_t = density of the recombination centers.

Recombination of excess carriers occur at these centers. High energy radiation can cause additional centers,this results in lattice displacements and vacancies that drastically shortens the carrier lifetime.

B. CARRIER TRANSPORT

There are two mechanisms that enable carrier transport or current flow to occur in semiconductors, drift current, and carrier diffusion. The drift current as related to holes in a p- material can be described by the following equation:

$$J_p = q\ p\ \mu_p\ E, \quad (2.10)$$

where J_p = hole current density (amps/cm^2)

q = hole charge (coulomb)

p = hole concentration (cm^{-3})

μ_p = hole mobility (cm^2)

E = electric field (V/cm)

The resistivity of the semiconductor material, ρ (ohm-cm), can be obtained from the following expression:

$$\rho = (q\ p\ \mu_p)^{-1} \quad (2.11)$$

Carrier diffusion is a process that results from random thermal movement of particles that exist in a concentration gradient. A hole flux will flow opposite to a gradient in the concentration of holes in a semiconductor. Thus an equation for the hole current density, given one-dimensional geometry, will be:

$$J_p = -q\ D_p\ dp/dx, \quad (2.12)$$

where J_p = hole current density (A/cm^2)

q = hole charge (coulomb)

D_p = hole diffusion constant (cm^2/sec)

dp/dx = gradient of hole concentration.

When both drift current and carrier diffusion are taken into consideration the following two equations can be written for hole current density, J_p, and electron current density, J_n:

$$J_p = q\,[p\,\mu_p\,E - Dp\,dp/dx], \quad (2.13)$$

$$J_n = q\,[p\,\mu_n\,E - Dp\,dn/dx], \quad (2.14)$$

Total current density can be obtained by taking the sum of equations 2.13 and 2.14.

C. DC MODEL THEORY

A non-illuminated piece of silicon, containing a p-n junction, is a good starting point for the development of a solar cell model. Figure 2.1 shows a schematic cross section of a solar cell containing a p-n junction. As discussed earlier the p- and n-material were created by doping the silicon material with Group III and Group V elements respectively. Therefore the p-material has a net positive charge while the n-material has a net negative charge. [Ref. 7]

The transformation from the p-material and the n-material occurs in a region called the transition zone. This region is less than 1-μm thick. The transition zone contains the p-n junction. This idealized concept does not actually

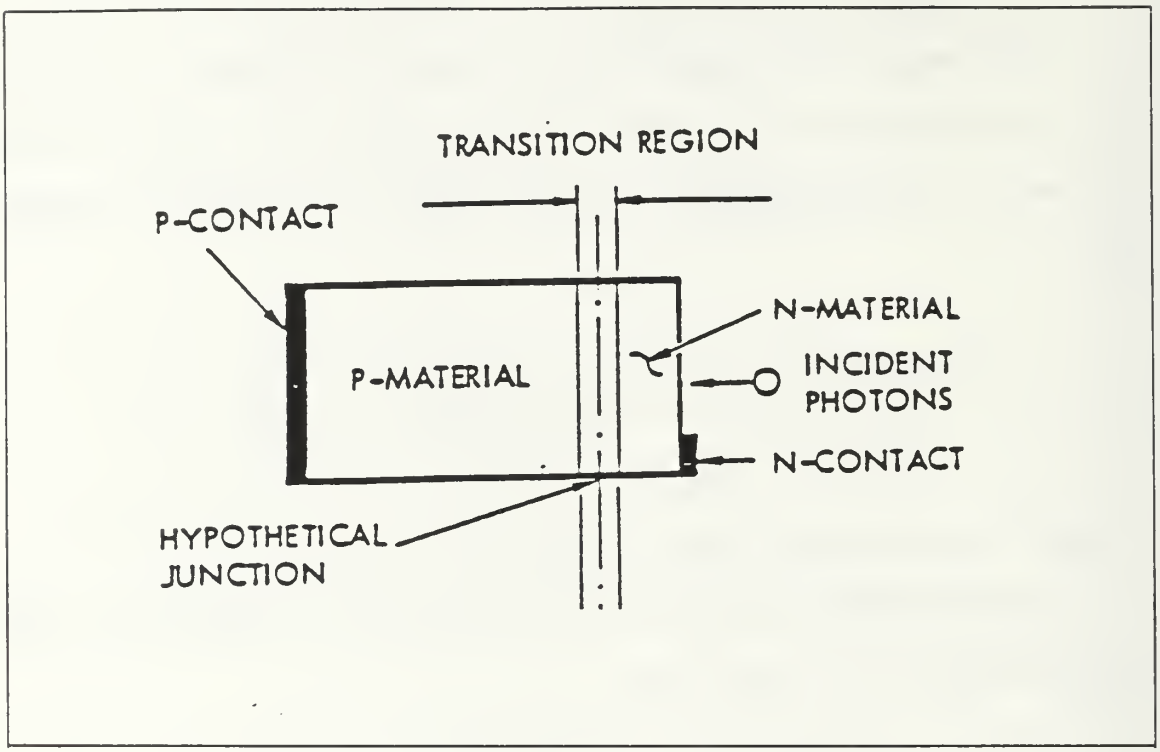

Figure 2.1 Cross Section of Solar Cell

represent a discrete line where the change-over from p- to n-material takes place. The process is a gradual change over a small area.

Thermal activity takes place in the atomic lattice at temperatures above 0° K. This thermal activity generates a random movement of holes and electrons in the p- and n-material. The doping process causes a much greater concentration of holes in the p-material and a much greater concentration of electrons in the n-material (Figure 2.2). These differences in concentrations in the p- and n-material have given rise to the term majority and minority carriers. In the p-material the holes are the majority carriers and the

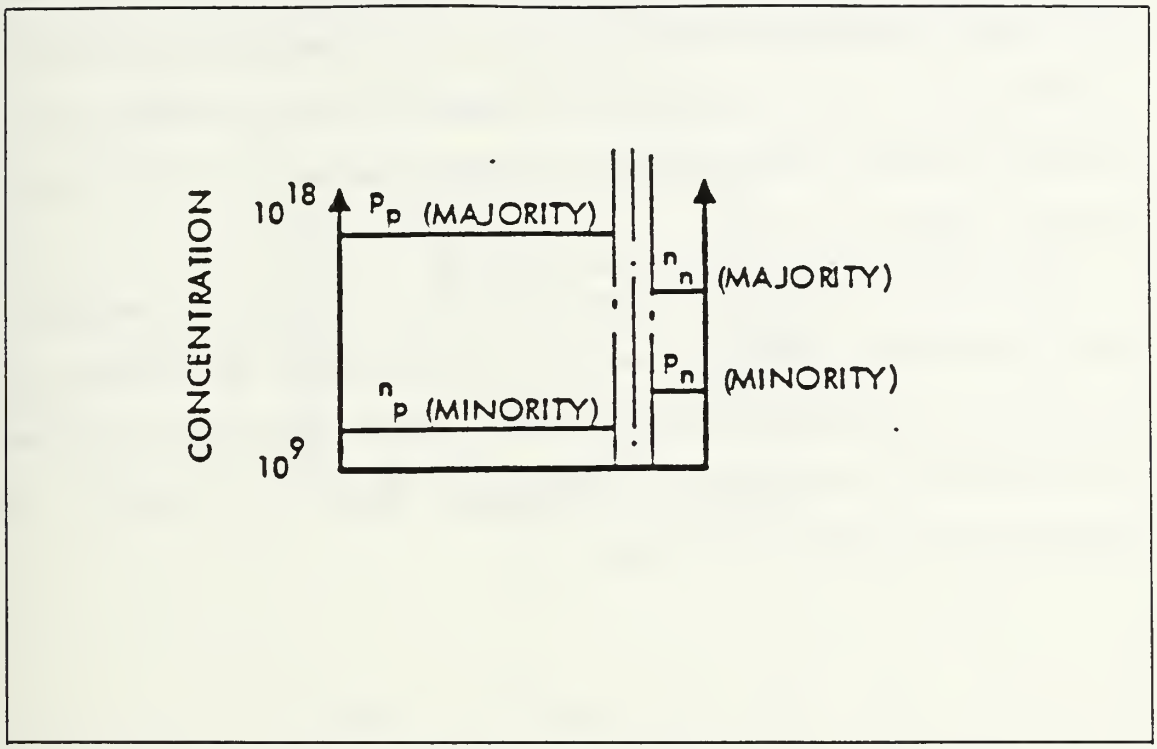

Figure 2.2 Hypothetical Concentrations of Holes and Electrons in a Solar Cell

electrons are the minority carriers. In the n-material the inverse is true. The behavior of the minority carriers is important in the operation of solar cell, therefore the solar cell is called a minority carrier device. [Ref. 7]

The excess concentration of holes and electrons on their respective sides of the p-n junction causes a hole density gradient, dp/dx, and a electron gradient, dn/dx, across the transition zone. The hole density gradient causes the holes to diffuse from the p-region to the n-region. The diffusion of electrons from the n-region to the p-region is caused by the electron density gradient (Equations 2.10-14).

As the distance away from the transition zone increases the actual concentrations of holes and electrons decrease (Figure 2.3). This pattern is caused by the process discussed earlier, recombination, electrons being acquired by holes. [Ref. 7]

The term minority carrier lifetime is used to describe the time period between the time an electron is injected and the time it recombines with a hole. The distance it travels during that time period is called the diffusion length. The equation for diffusion length is:

$$L_p = (D_p \tau_p)^{1/2} , \quad (2.15)$$

where D_p = diffusion constant (Eq. 2.12)

τ_p = lifetime of hole (Eq. 2.7)

In solar cells the sun's electromagnetic radiation (photons) is used as the motive force to inject minority carriers into the solar cell. The incoming photons must have enough energy to produce excess charge carriers, thus forming an electron-hole pair in the semiconductor material. These carriers cross the diode potential barrier and set up an electrical current that can be used as an energy source (Figure 2.4). The term injection level is used to refer to the number of photons incident upon a unit area in a given time.

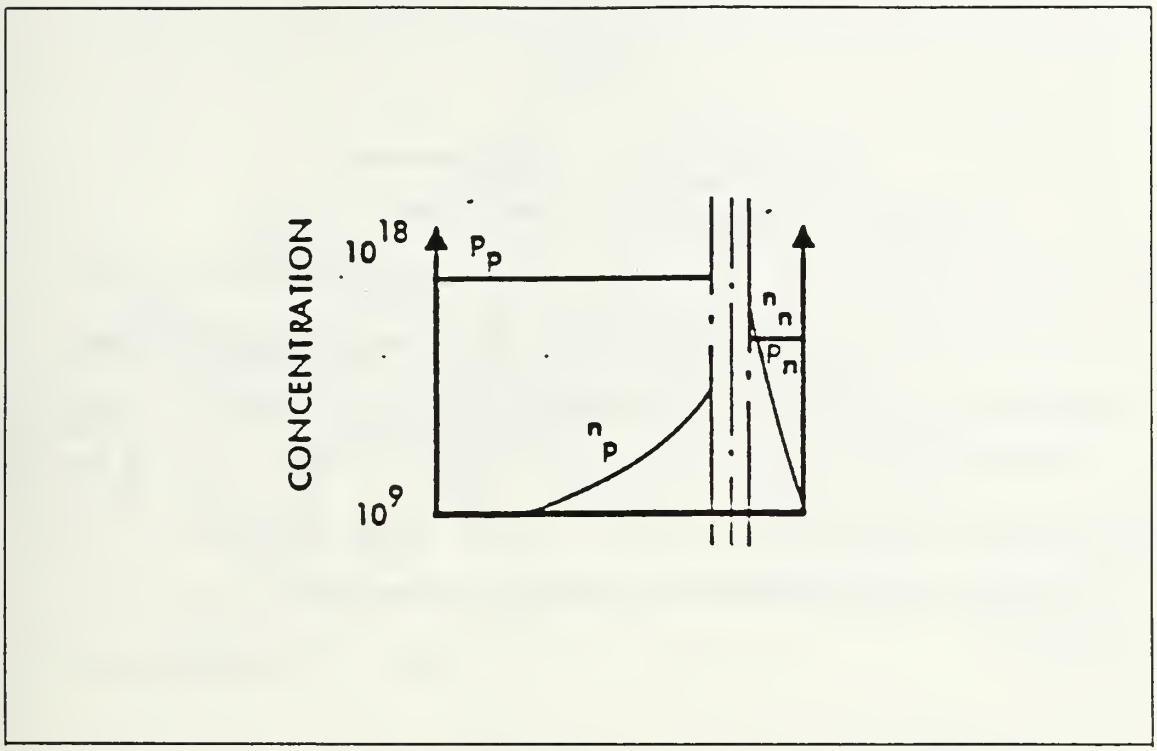

Figure 2.3 Actual Concentration of Holes and Electrons

Solar cells are very selective devices. The only photons that a given device will use to convert to a usable energy is one whose energy exceeds the band gap between the ground state and the excited state of its electrons. Since photon energies are inversely proportional to wavelength, these energies are spread out over a wide range of values. An average silicon solar cell has a bandgap of 1.2 eV therefore only that part of the Sun's spectrum that has photons with wave lengths less than 1 micrometer will be absorbed. Those photons with energy less than 1.2 eV will pass through the device. Photons with energy greater than 1.2 eV that are absorbed by the device will only release 1.2 eV of recoverable

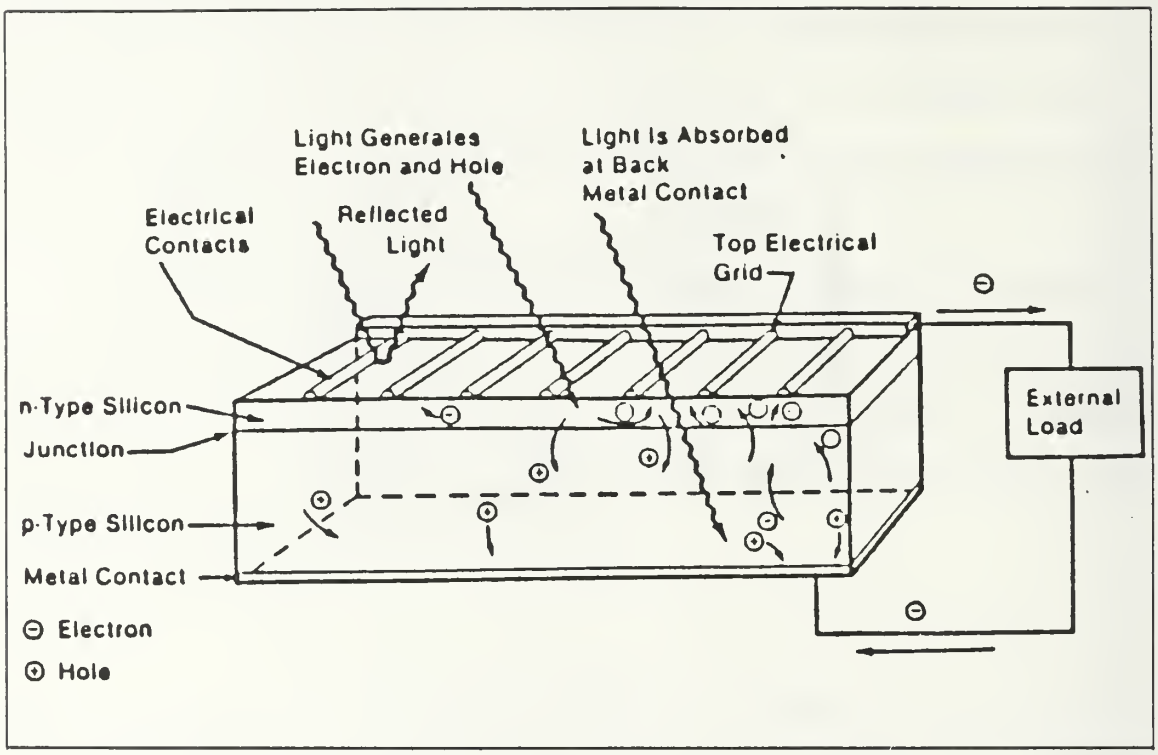

Figure 2.4 Light Incident on Cell
Creates Electron-hole Pairs

energy to the solar cell, the excess energy will be dissipated as heat. Most solar cells have band gaps between 0.1 and 4 eV.

As discussed previously the carrier diffusion across the transition zone provides high concentrations of free electrons (from the n-side) the ability to recombine with holes (from the p-side). This process causes the donor and acceptor ions to be depleted in the transition zone. This has led the transition zone to be called the depletion region (Figure 2.5). [Ref. 7]

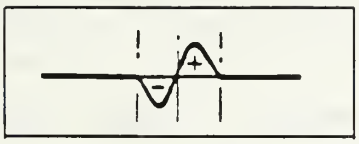

Figure 2.5
Charge Density in Depletion Region

An electrostatic potential is built up in this region due to the immobile ions. This potential opposes the diffusion currents. This potential barrier, V_o, (Figure 2.6) allows holes (solid line) in the n-material to drift to the p-material and electrons (dashed line) to move from the p-side to the n-side. This was discussed earlier in the Carrier Transport section, Equation 2.10. [Ref. 7]

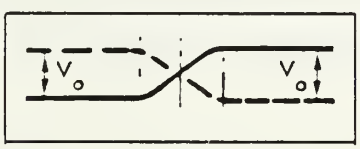

Figure 2.6
Electrostatic Potential in Solar Cells

The principle of conservation of charge must be satisfied when the equilibrium of diffusion and drift currents occur (at any time, t, and at a given distance, x, from the p-n junction). The conservation of charge equation can be written as follows for holes in the n-material.

$$\frac{\partial p_n(x)}{\partial t} = \frac{-p_n(x) - p_{no}}{\tau_p} + D_p \frac{\partial^2 p_n(x)}{\partial x^2} - \mu_p \frac{\partial [p_n(x) V_o]}{\partial x}, \quad (2.16)$$

Equation 2.16 states that the increase in minority carrier hole concentration in the n-material (related to the distance, x, with respect to time ;the left side of the equation) is equal to the externally injected hole concentration (caused by light or voltage bias) minus the thermal equilibrium concentration, p_{no}, (first term right-hand side) plus the contributions of the diffusion and drift currents (second and third terms). [Ref. 7]

Two boundary conditions are required to solve the above equation. One is that the injected hole concentration decreases away from the junction of $p_n(x) \to 0$ as $x \to$. The other boundary condition is that the hole concentration $p_n(0)$ at the junction, depends on the minority carrier p_{no} and the externally applied voltage, V, according to:

$$p_n(0) = p_{no} \exp(eV/kT), \quad (2.17)$$

The solution of the continuity equation with the boundary conditions, gives us the dc diode equation:

$$J_D = J_o \{\exp(eV/kT) - 1\}, \quad (2.18)$$

where $J_o = q D_p p_{no}/L_p + q D_n n_{po}/L_n$.

When a solar cell is illuminated the continuity equation generates another term which represents the "light injected" minority carrier concentrations (i.e., the holes in the

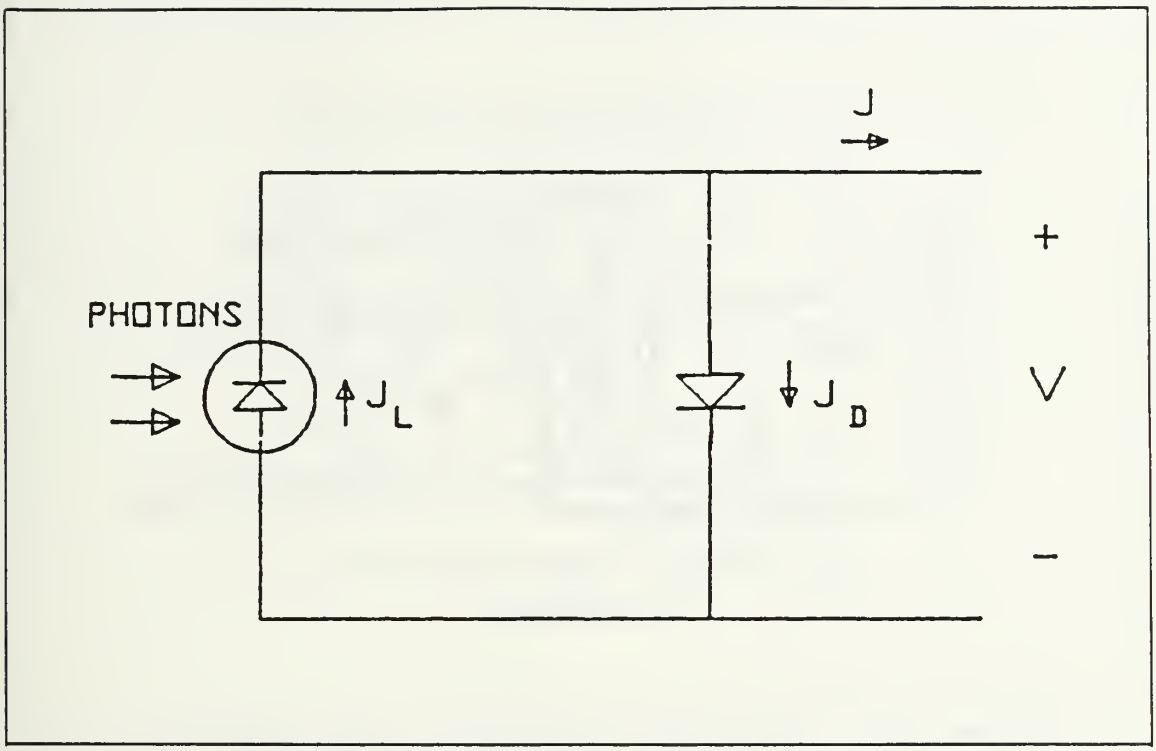

Figure 2.7 Solar Cell Equivalent Circuit

n- region). These light generated minority carriers give rise to the current density, J_L (light generated), which is available as current in an external circuit. The complete solar cell equation is then as follows:

$$J = J_L - J_o \{\exp(eV/kT) - 1\}, \quad (2.19)$$

For this equation an idealized circuit can be synthesized as shown in Figure 2.7. The current source produces (via photons) a current J_L equal to the injection level while the total value of the cells current is the difference of J_L - J_D.

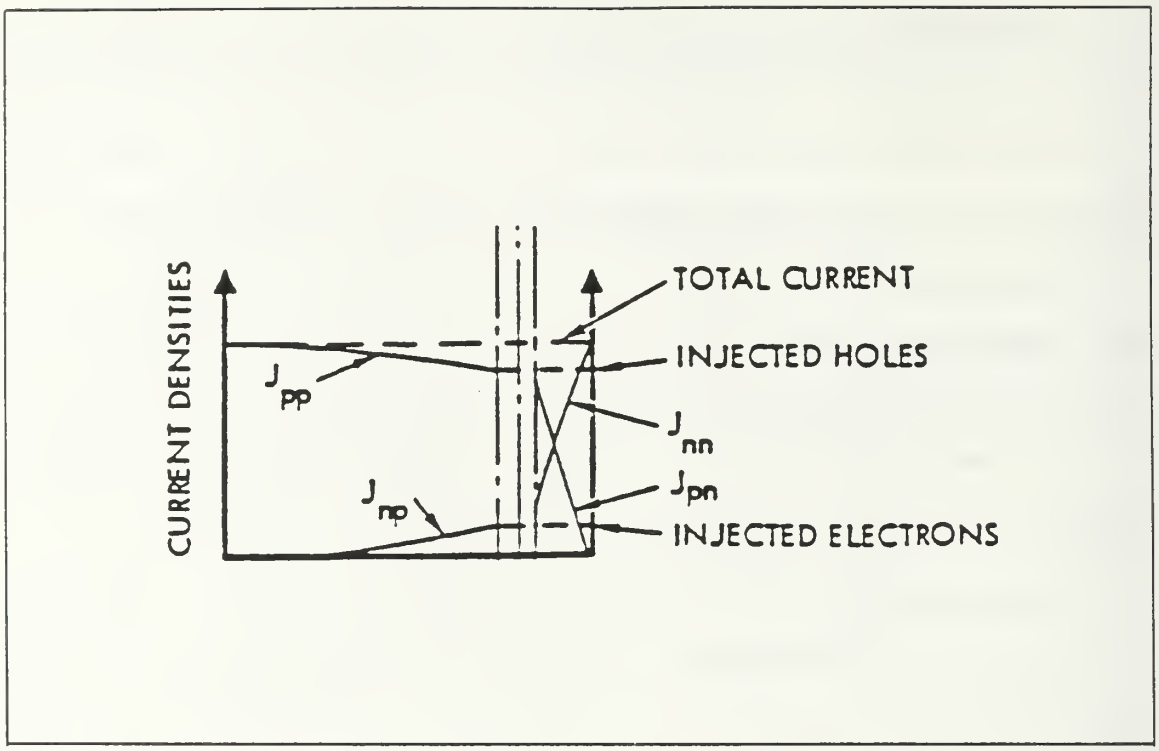

Figure 2.8 Hole and Electron Current Densities

In Equation 2.16 the quantity, $p_n(0)$, represents the concentration of holes in the n-region and can be caused by either an external forward bias or by minority carrier holes generated by photons. When the junction is forward biassed (by an external voltage or by photons) the internal electric field (Figure 2.4) causes holes to drift from the p-side to the n-side. When the hole drift current crosses the junction, it becomes an injected hole current in the n-region. The reverse is true for the electron current in the n-region, it becomes an injected electron current in the p-region. The sum of the hole-electron currents at a distance, x, equal the total current density, J (Figure 2.8). In Figure 2.8 J_{pp} is equal to the hole drift current; J_{np} is equal to the electron

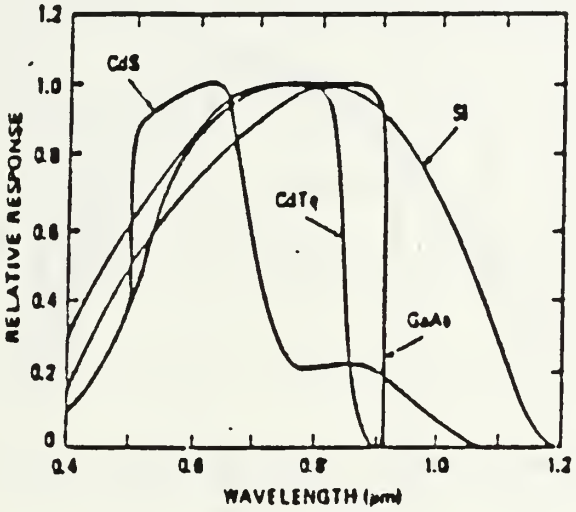

Figure 2.9 Spectral Response of Several Semiconductor Materials

diffusion current (injected minority carriers); J_{nn} is equal to the electron drift current; and J_{pn} is equal to the hole diffusion current (injected minority carriers).

As the holes approach the junction (J_{pp} in Figure 2.8), some of them recombine with the injected electrons (J_{np}), thereby lowering the total current density, J. [Ref. 7]

D. IMPROVEMENTS IN SOLAR CELLS

Improvement of solar cell efficiency can be accomplished in three major areas, choice of materials (Si,GaAs,etc), choice of material parameters (doping levels), and configuration (junction depth and surface contact patterns).

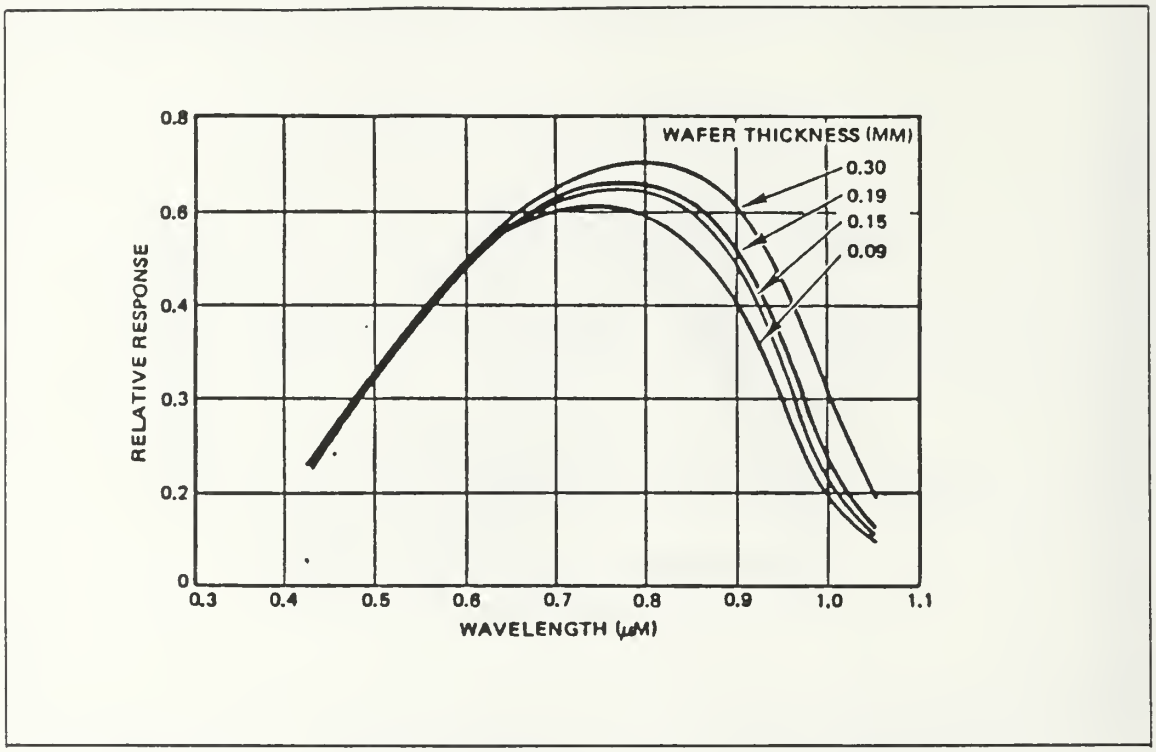

Figure 2.10 Change in Spectral Response Due to Cell Thickness

The choice of a material whether, Silicon or Gallium Arsenide, is determined by a variety of considerations. The ability of a manufacturer to process the material at reasonable costs can play a major role in determining which material is chosen. The physical properties of the material must be such that the absorption coefficient and energy gap are sufficient for efficient photovoltaic operation (Figure 2.9).

The depth of the junction and thickness of cell will affect the cells ability to absorb light which will influence the cells output (Figure 2.10). In the diffusion process a relatively large atom such as phosphorus can cause structural

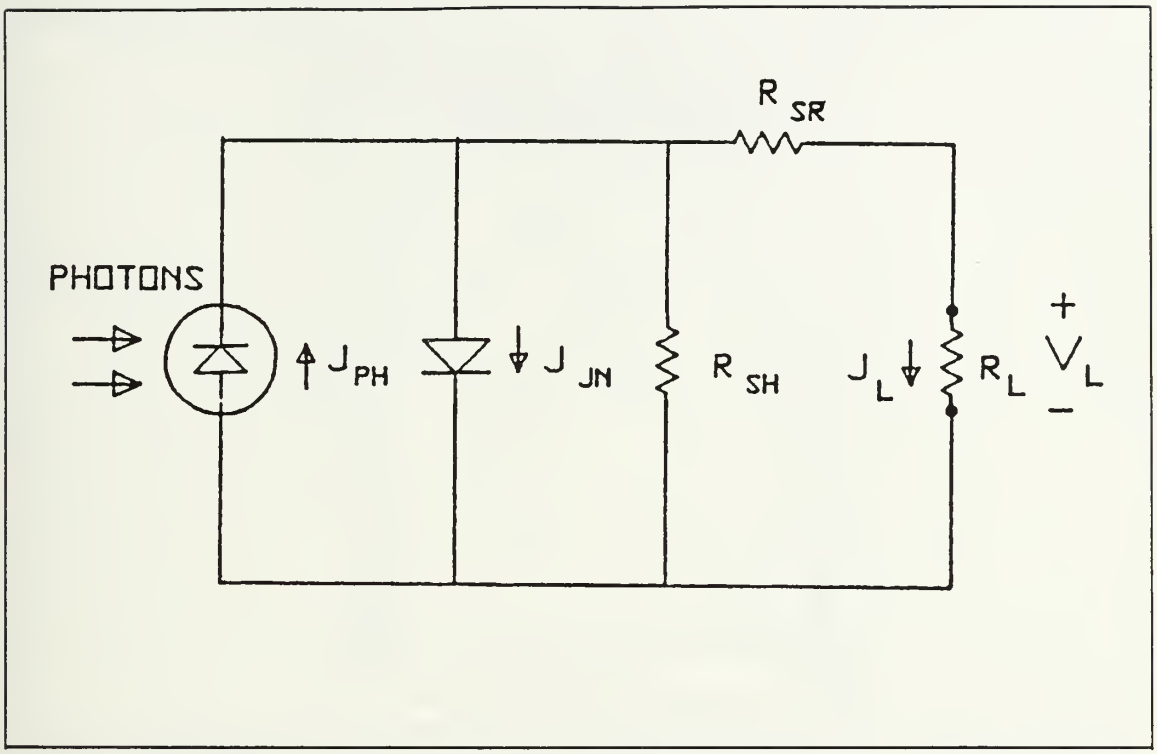

Figure 2.11 Modified Solar Cell Equivalent Circuit

defects in the crystal lattice. Configuration of front and back contacts can change the series resistance and the surface recombination velocity.

The recombination velocity can be altered by changing the dopant levels. A type of cell known as the Back Surface Field cell is created by doping the p-material at the rear of a cell so that it becomes a p(+)-material. This reduces the recombination rate at the rear to almost zero.

With the knowledge of what affects a cell's performance, a better equivalent circuit can be developed. Using Figure 2.11 as a starting point, we can add some components to the

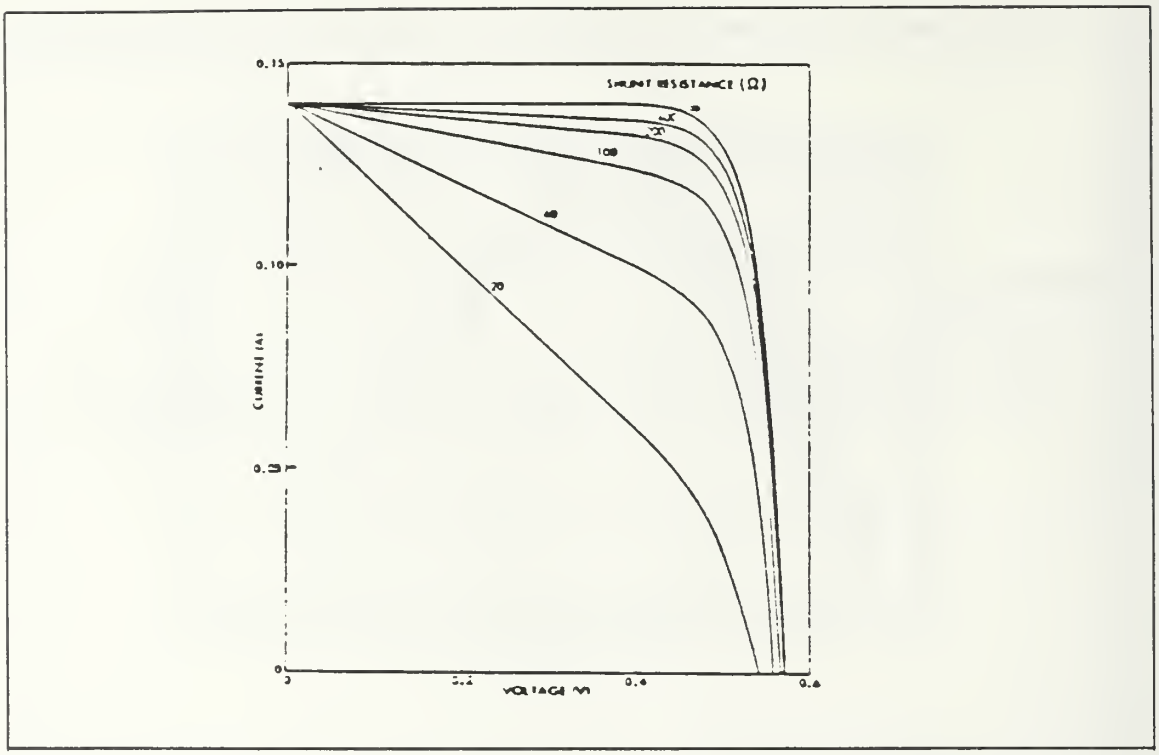

Figure 2.12 Effect of Shunt Resistance on I-V curve

circuit so that we can model the changes of solar cells when we change properties and parameters. [Ref. 4]

Figure 2.11 shows a photon excited current, J_{ph} that is produced when the cell is illuminated. Some of this current is lost via the flow of electrons back through the junction, J_{jn}, or is lost via shunt paths (shunt resistance, R_{sh}) across the junction. Non-perfect contacts and high sheet resistances can cause losses that are lumped under series resistance, R_{sr}. Shunt resistances can be caused by surface leakage around the cell and improper manufacturing processes such as faulty diffusion techniques and crystal defects. Series resistance can be caused by ohmic resistances in the

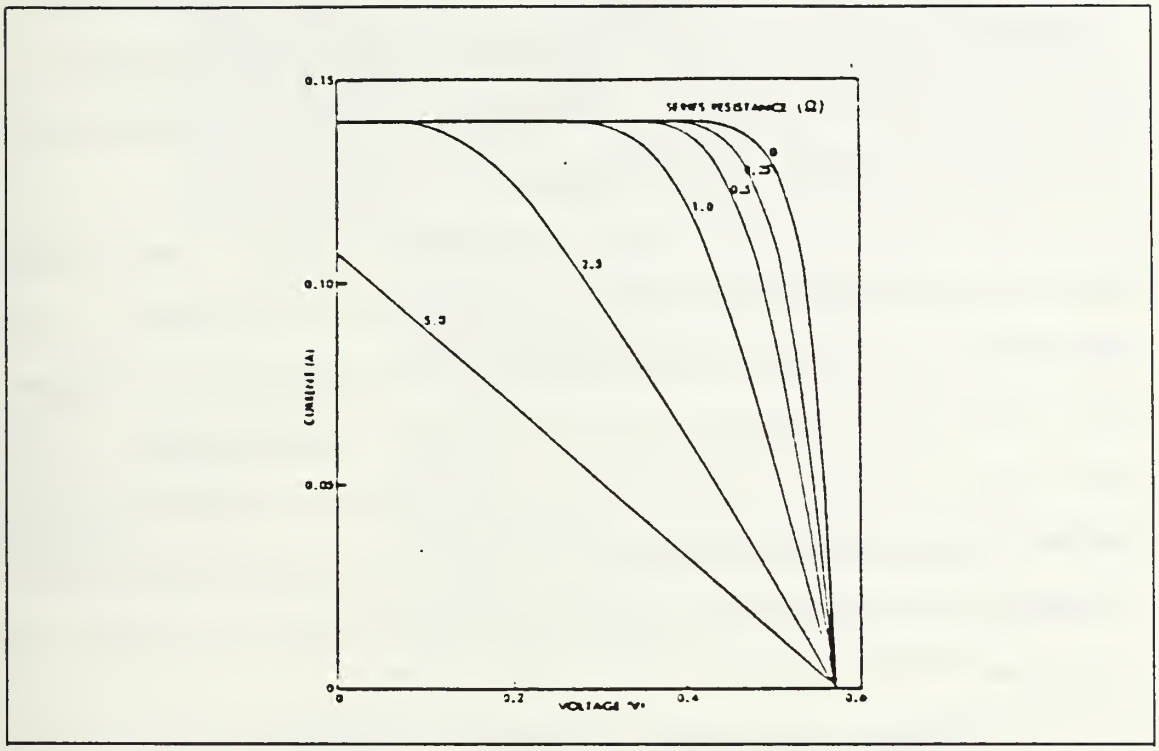

Figure 2.13 Effect of Series Resistance on I-V Curve

contacts, the base resistivity of the base material and the sheet resistance of the diffused layer. Figures 2.12 and 2.13 show what the changes in the respective resistance will cause in the I-V curve.

These figures show that to improve solar cell efficiencies, the manufacturer must increase the shunt resistance so that it approaches infinity and decrease the series resistance to approximately zero. [Ref. 7]

E. DAMAGE TO SOLAR CELLS

The major damage to solar cells occur in space and is caused by radiation damage. Though some damage can occur on

earth, these damages (moisture and physical damage) are generally prevented form occurring by the manufacturers quality control process. Therefore we will concentrate on the damage caused by radiation.

The change in the output parameters can be used to describe solar cell behavior in a radiation environment. This approach limits the understanding of the physical changes that the cell undergoes during radiation bombardment. Since the space arrays of the future may exist in complex environments, using exotic materials, a good understanding of how radiation interacts with matter is required by the solar cell designer.

1. Radiation Damage Theory

The solar cell designer's interest, is the study of degradation of materials and devices caused by high velocity, massive particles (electrons, protons, neutrons, or ions). These particles have mass, energy, and possibly charge and therefore interact with material in several ways.

The dominant interactions are [Ref. 6]:

(1) Inelastic Collisions with Atomic Electrons. These collisions with bound atomic electrons are usually the predominant mechanism by which an energetic charged particle loses kinetic energy in an absorber. This will either cause the electron to experience a transition to excited state (excitation) or to an unbounded state (ionization).

(2) Elastic Collisions with Atomic Nuclei. Charged particles may have coulombic interactions with the positive charge of the atomic nucleus. In some cases this interaction may have enough energy to displace it from its position in a crystalline lattice. This can cause the displaced atom to undergo collisions with other atoms in the lattice structure.

(3) Inelastic Collisions with Atomic Nuclei. The process spalation falls under this category. This process, which is important to cell designers, occurs when an energetic proton interacts with the nucleus and leaves the nucleus in an excited state. The excited nucleus emits energetic nucleons and the recoiling nucleus is displaced form its lattice site. This displaced nucleus can then cause more displacements.

There are two major types of radiation damage that cell designers are interested in, ionization and displacement.

a. Ionization

Ionization occurs when orbital electrons are stripped from an atom or molecule. Radiation may effect solar arrays by several ionization related effects. The reduction of transmittances in solar cell coverglass, increased leakage currents are some of the effects of ionization.

Ionizing radiation creates electron-hole pairs in silicon (exciting the electrons of the valence band to the conduction band) in much the same way that carrier pairs are generated by visible light. Three times the amount of energy must be absorbed from a high energy particle to produce the same carriers that an optical photon of energy would create.

b. Atomic Displacements

The energy loss by high velocity particles caused by collision processes with the electrons of an absorber or target material accounts for a large fraction of the dissipated energy. This damage is caused by the

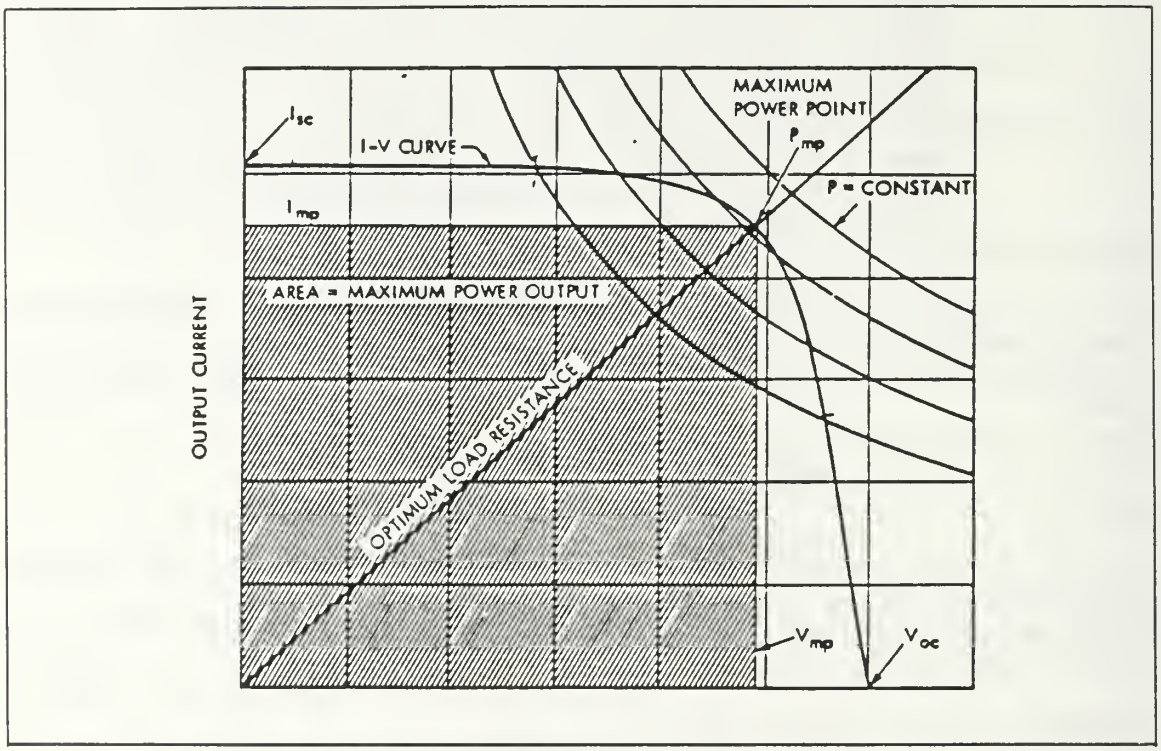

Figure 2.14 Example I-V Curve

displacement of silicon atoms from their lattice sites by fast particles in the crystalline absorber. The displaced atoms form stable crystal defects which produce significant changes in the equilibrium carrier concentrations and the minority carrier lifetime.

2. Silicon Solar Cell Damage

Solar cell damage is investigated by examining the changes in the cell's short circuit current (I_{SC}, Maximum current the cell can generate when it's two terminals are short circuited), open circuit voltage (V_{OC}, voltage across the cells terminals when circuit is not loaded), and maximum power point (P_{mp}, power at the knee of the I-V curve, Figure 2.14). Basic solar cell equations can be used to describe

the changes that occur during irradiation. Though some investigations have reported variations in these equations, not enough data has been collected to determine the significance of the variations.

Diffusion length is also used to measure the damage that occurs in a solar cell. Problems can arise using this method since very low energy protons do considerable displacement damage within the junction space charge region of a solar cell. Even though the diffusion length of the cell has not been changed, this damage can cause serious reduction in solar cell I_{SC} (Figure 2.15). Use of the diffusion length has other difficulties as well, the relationship between diffusion length and the solar cell output parameters is not well defined, diffusion length is more difficult to measure than cell output parameters, and accurate measurement of diffusion length of thin cells is extremely difficult.

Because of these problems, an empirical method has evolved to evaluate the degradation of solar cells (caused by irradiation) in terms of common engineering output parameters. The variation of common solar cell output parameters during irradiation can be describe as:

$$I_{SC} = I_{SC}(0) - C \log[1 + \phi/\phi_X \,], \quad (2.20)$$

where ϕ_X = radiation fluence at which I_{SC} starts to change to a linear function of the logarithm of the fluence.

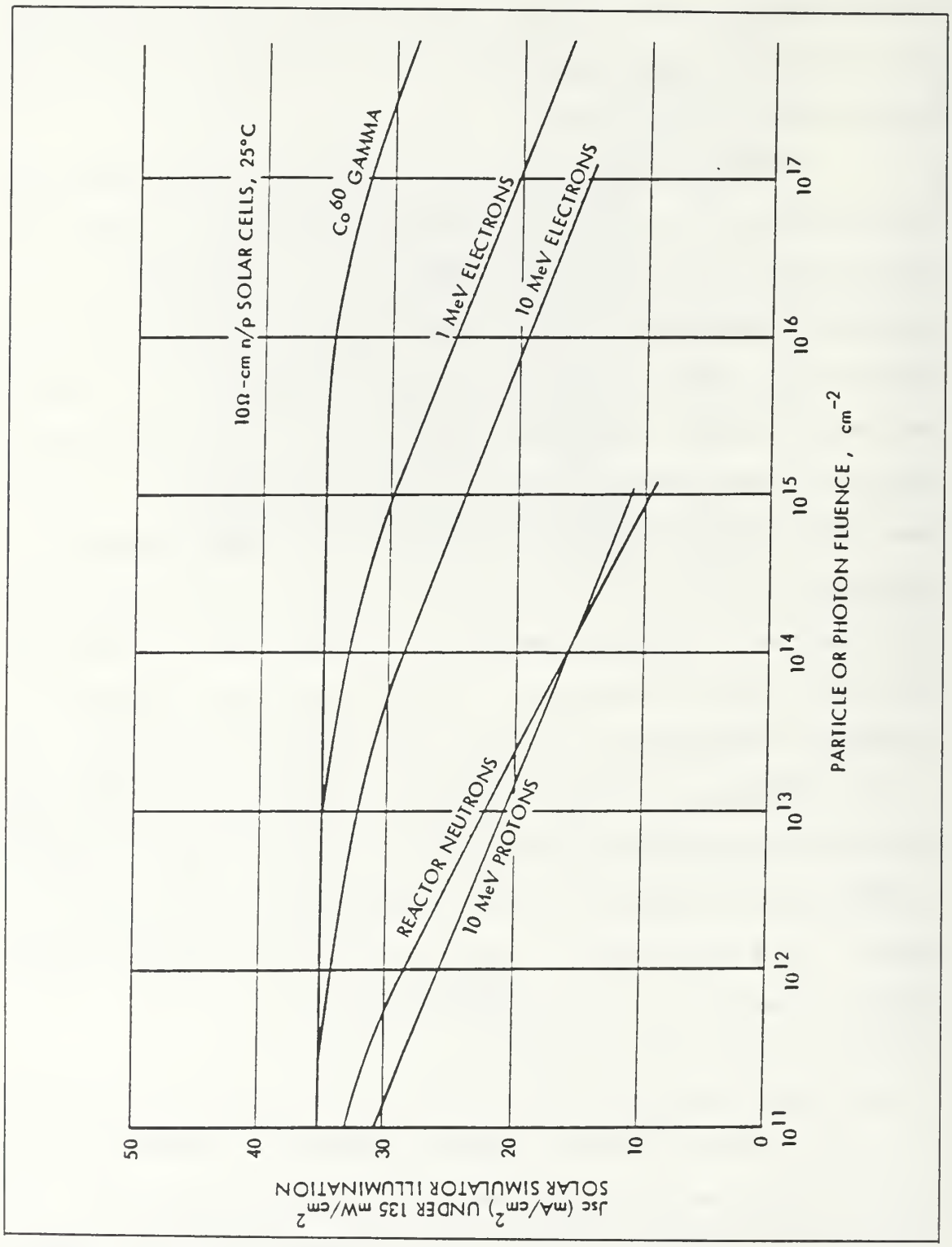

Figure 2.15 Variation in I_{sc} for Various Radiations

C = decrease in I_{SC} per decade in radiation fluence in the logarithmic region (this constant does not vary much for different radiation environments, Figure 2.15).

3. Concept of Damage Equivalence

Since there is a broad range of high velocity energies present in the space environment it has become necessary to describe the effects of these various energies in terms of a radiation environment which can be simulated under laboratory conditions.

Since 1 MeV electrons are a common and significant component of space radiation and because they can be produced conveniently in a test environment, they have been used as a basis of the damage equivalent fluences which describe solar cell degradation.

This damage equivalent fluence method causes two separate problems. The first problem is to develop a method in which an accurate model for the degradation of an unshielded solar cell (under 1 MeV electron irradiation during laboratory conditions) can be described. The second is to have the ability to reduce the effect of the space radiation environment on a shielded solar cell to the damage equivalent fluence achieved in laboratory conditions.

Damage equivalence for protons is based on 10 MeV proton fluences. The equivalent 10 MeV proton fluence can be converted to equivalent 1 MeV electron fluence as follows:

$$\phi_{(1\ \text{MeV e})} = 3000 \cdot \phi_{(10\ \text{MeV p})}, \quad (2.21)$$

This relationship is an approximation which must be made for the purpose of combining electron and proton damage.

4. Irradiation of Silicon Solar Cells

Currently the primary power source on nearly all earth orbiting satellites are n-on-p solar cells. Modification in base resistivity and cell thickness can cause significant differences in the cell's ability to resist degradation. Variables such as the environment temperature in the range of 200 to 300°K, and p-type dopants have been shown to have little or no effect on the solar cell's response to radiation.

Choice of the solar cell material (base resistivity) can affect the efficiency and the radiation resistance of the cell. As the base resistivity increases the efficiency decreases and the radiation resistance increases. Finding the best base resistivity can be accomplished by finding the point where the absolute cell output is greatest after a given radiation dose.

Current n/p cells have confined resistivity to ranges of 1 to 3 ohm-cm and 7-13 ohm-cm. Cells in the lower ranges have greater initial power output but are less resistant to radiation than the 7-13 ohm-cm range cells.

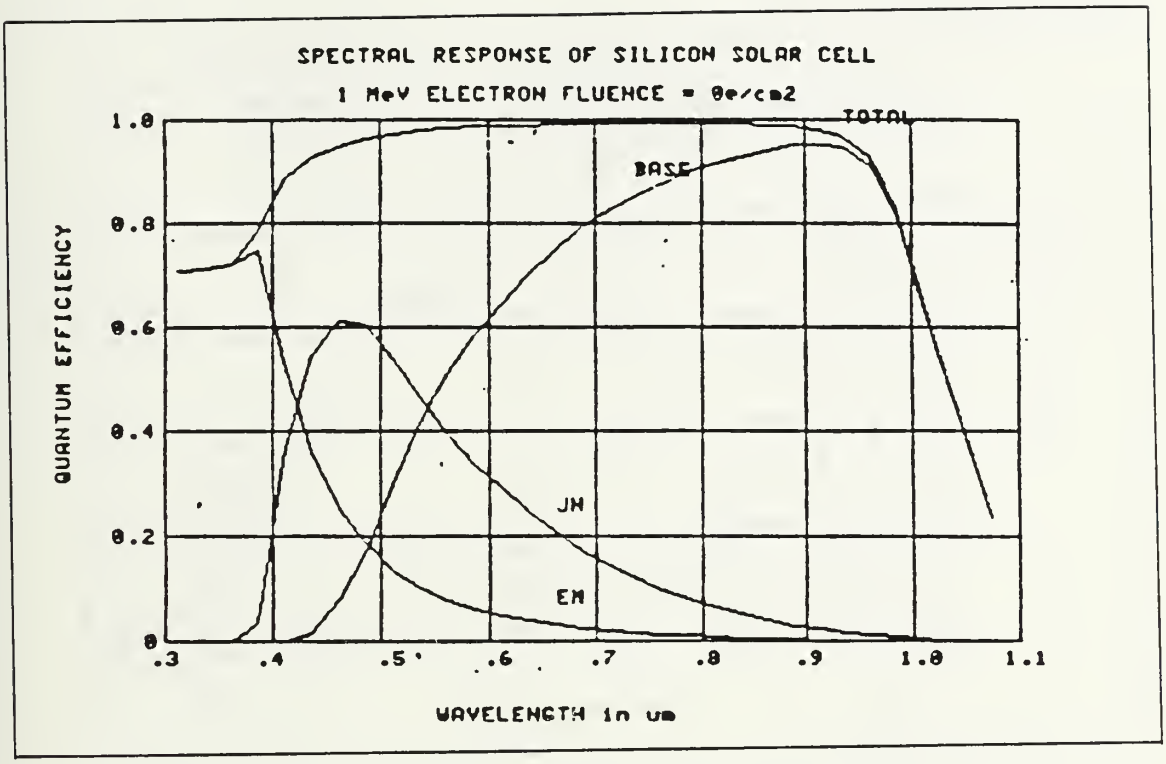

Figure 2.16 Spectral Response of a Silicon Cell; Nonirradiated

Figures 2.16 and 2.17 show a pictorial description of what happens to a silicon cell that has been irradiated with 1 MeV electrons. Figure 2.16 displays the spectral response of a solar cell before irradiation. Note that the base has the majority of its response in the red portion of the spectrum.

Figure 2.17 demonstrates the effect that radiation has on the red response of a silicon solar cell. Again note that almost all of the degradation occurs in the base material.

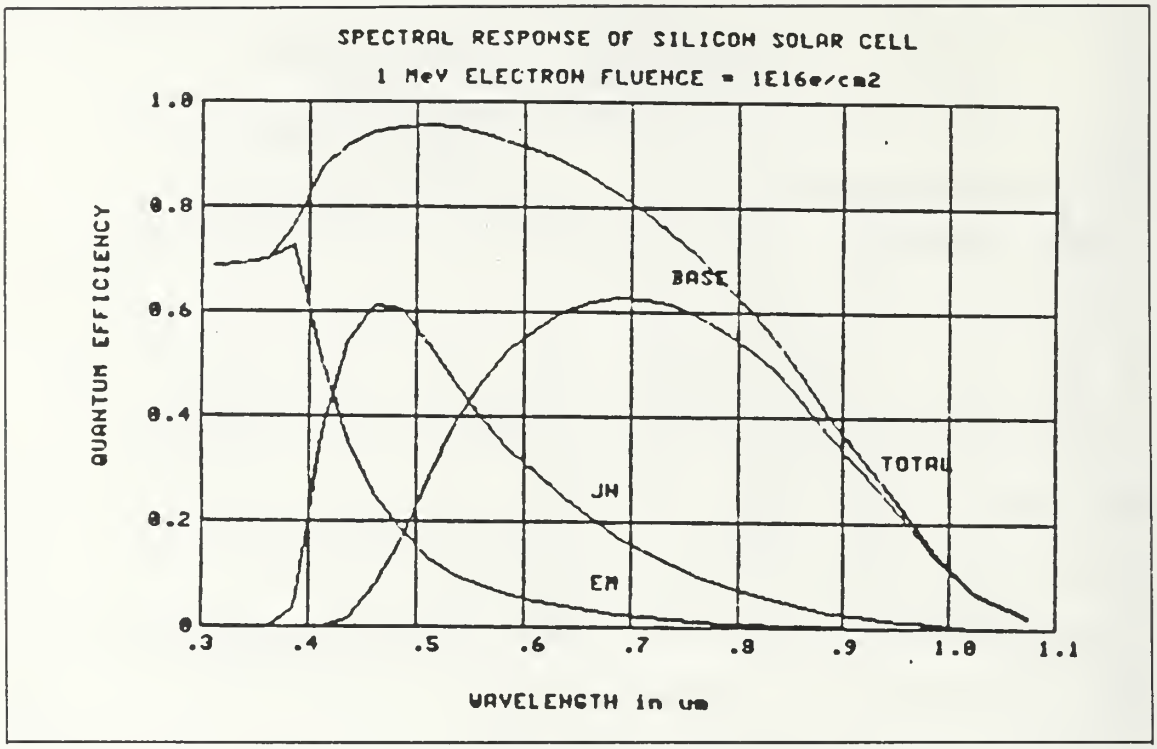

Figure 2.17 Spectral Response of a Silicon Cell; Irradiated with 1 MeV Electrons

5. Solar Cell Degradation, Electrons

A method for evaluating the damage effectiveness of electrons of various energies is required so that the concept of damage equivalent 1 MeV electron fluence can be used effectively. This effectiveness can be measured by the solar cell critical radiation fluence (ϕ_c). Critical fluence is defined as the fluence which will degrade a cell parameter to a certain value. [Ref. 6]

Using experimental data, one can define a relative damage effectiveness for each electron energy which will be a measure of the ratio of that electron fluence at a given

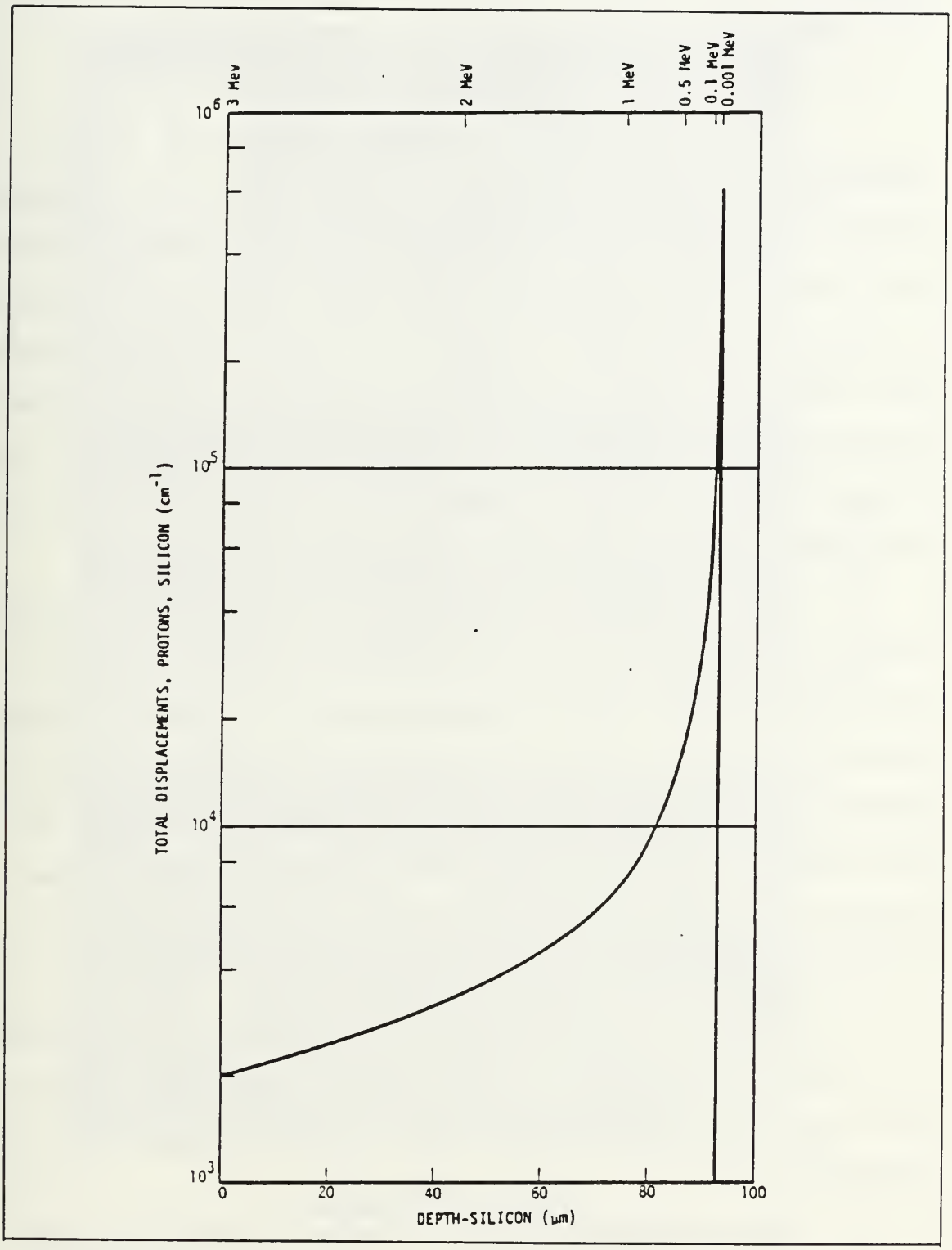

Figure 2.18 Atom Displacements as a Function of Depth (3 MeV Proton in Silicon)

energy to the 1 MeV electron fluence necessary to degrade an n/p solar cell to the same output parameter value.

6. Solar Cell Degradation, Protons

While the concept of damage equivalence can be extended to proton irradiation, the problem is more complex. Protons produce nonuniform damage because the range of protons below 5 MeV is less than the usual solar cell thickness. A complication is caused by the fact that the damage produced per unit path length increases as the proton energy decreases (Figure 2.18). Protons in the energy range from 1.5 to 3 MeV produce maximum radiation damage in silicon solar cells. The degradation is more severe to V_{oc} and P_{mp} than to I_{sc}.

Proton damage in silicon solar cells can be normalized to the damage produced by protons of a single energy. The proton energy used for normalization of relative damage should be close to that which produces the maximum damage in space environments. This energy must produce relative uniform damage, and be available for laboratory evaluations. The use of 10 MeV proton damage is a compromise of the requirements listed.

Figure 2.19 shows relative damage results normalized to 10 MeV proton damage. These results have been shown to hold for both 10 ohm-cm and 2 ohm-cm silicon solar cells at energies greater than 10 MeV. [Ref. 6]

The alteration of silicon solar cell output parameters with 10 MeV proton fluence is similar to that

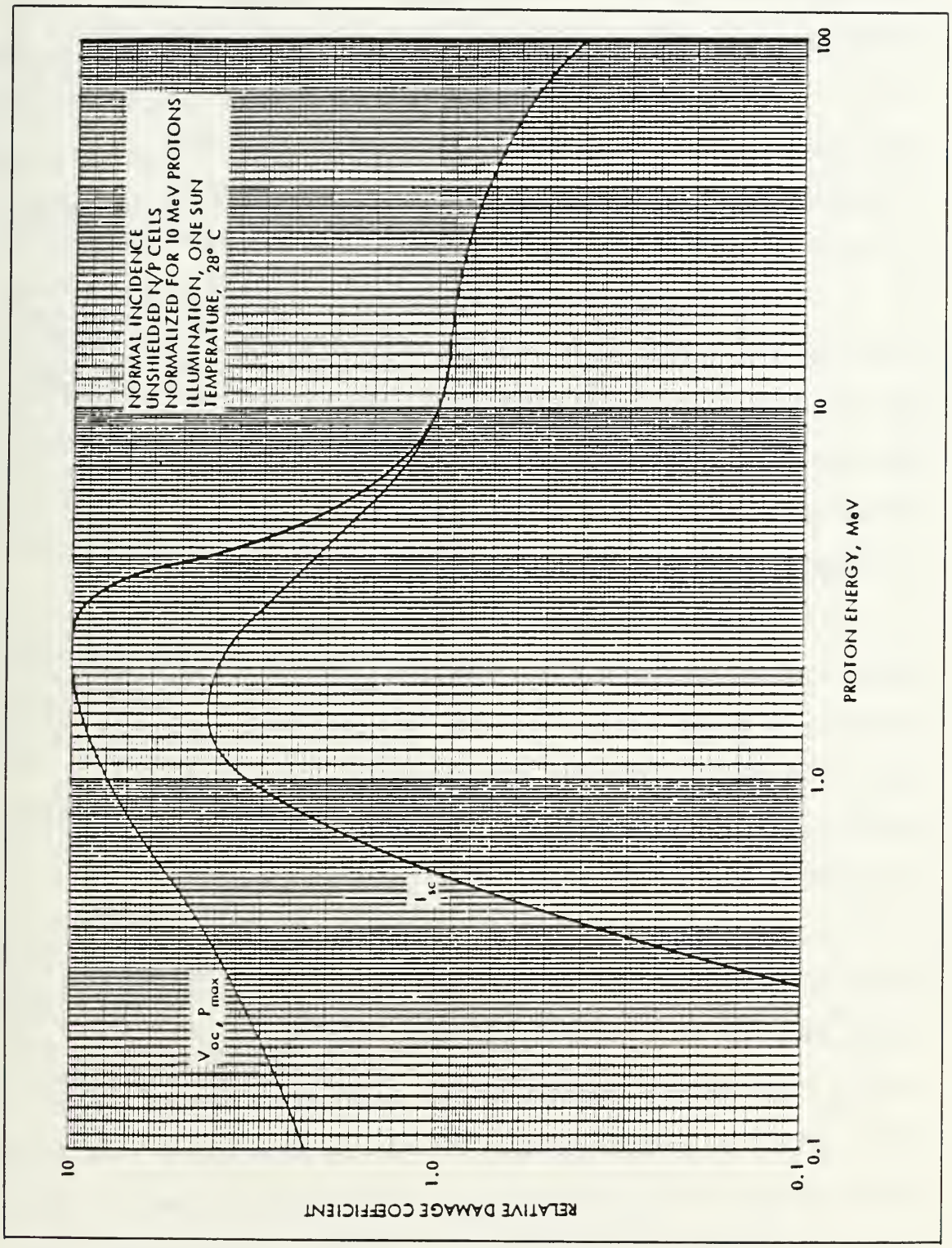

Figure 2.19 Relative Damage Coefficients for Proton-Irradiated Silicon Cells

discussed previously. The values of constants tend to be somewhat greater than those found for 1 MeV electron irradiation. This difference between the constants implies that the concept of equivalency between the different types of radiation has its limitations and is basically an approximation.

7. Junction Damage (Low Energy Protons)

Low energy protons can affect the unshielded portions of the solar cell. These unshielded areas are very small (in the micrometer range) and usually occur because of improperly placed coverglass. As was discussed in the previous section low energy protons have a greater effect on V_{oc} and P_{mp} than electrons or high energy protons.

Studies of satellite power systems have shown that small unshielded areas can cause significant degradation to an array's power output (ATS-1, a satellite launched in 1966 had a 20% degradation). Array manufacturers have taken measures to cover all areas of the cells front surface with coverglass and to fill any gaps with adhesive.

This degradation of power can be explained in terms of solar cell theory. Since the range of low energy protons in silicon is limited to less than the cell thickness, particles that do not penetrate the cell cause defects only to their depth of penetration. It can be shown that the damage rises rapidly to a maximum as a proton gets closer to it's penetration depth (Figure 2.18). Protons which enter the silicon with energies of 0.5 MeV or less produce damage which is concentrated within a few microns of the cells surface.

The space charge region of a modern cell extends form 0.4 to 1 micron below the cell surface, thus damage is concentrated in the junction region [Ref. 6].

8. Radiation Damage Annealing

In general, the crystalline lattice damage and associated electrical degradation to solar cells caused by different radiations is not always stable. Annealing of damage occurs above 20 ^{o}C, and can increase a damaged cells output by as much as 5%. Temperatures of 100 ^{o}C and greater, accelerate this process but do not change the maximum level of 5%. The annealing process seems to be more significant for proton and neutron damage than for electron damage.

Some solar cells may experience a degradation or a recovery during subsequent long term illumination. Photon degradation is usually less than 1%, causing both a loss in the minority carrier lifetime and the cell's red response. Spectrolab has found that after an exposure of 1 X 10^{15}e-cm^{-2} of 1 MeV electrons some silicon solar cells had from a 0 to 5% recovery after 48 hours. "This leads us to the conclusion that lifetime is not a constant material property as heretofore assumed, but rather depends strongly on thermal and light exposure history of the material." [Ref. 9]

III. PHOTOVOLTAIC TESTING

A. HISTORICAL BACKGROUND

Since the development of the solar cell in the 1950's, solar cell measurement techniques have progressed from an initial volt-ohmmeter test in "fair weather" to high altitude and space experiments, sunlight simulators, accurate spectro-radiometric apparatus, and analog and digital data acquisition systems.

Originally, solar cells and solar cell assemblies for use on space vehicles were evaluated in the laboratory by measurement under incandescent illumination. Tungsten lamps with color temperatures of the order of 2700 to 3400 degrees Kelvin, compared to the greater than 6000 degrees Kelvin color temperature of the air-mass-zero sun were used to illuminate the cells.

In the 1950's it was already realized that measurement were not repeatable in tungsten unless the filament voltage, and hence the lamp, was closely controlled and the solar cell temperature was held within close tolerances.

In the early 1960's cells were tested in natural sunlight in normal outdoors conditions in an arbitrary intensity level of 100 mW/cm^2. When precision was required, solar cells were measured in essentially collimated sunlight and in other cases applying a correction based upon the ratio of short

circuit currents of a cell measured in uncollimated light to that of measured in collimated light accounted for the sky background. Having calibrated several such cells, these "standards" were then taken into the laboratory and used to adjust the intensity of tungsten illuminators [Ref. 7].

By thus calibrating solar cells under sunlight conditions which were more nearly reproducible and by maintaining control of the incandescent illumination, it was felt that sufficient accuracy could be achieved to permit adequate extrapolation of outputs to air-mass-zero conditions. However, in 1961 it was discovered that in the attempts to improve solar efficiencies the spectral response had been so significantly shifted toward the red as to introduce errors of as much 15 to 20 percent between the measured and predicted cell efficiencies. Thus, cells and panels made at the time were being measured under sources calibrated against standard cells of different spectral response, such that the cell and panel outputs appeared to be approximately 15 percent more efficient in space than was actually the case. As a result of this problem, considerable attention was focused by industry and government on the test methods. [Ref. 7]

During the following years, the development of solar radiation simulators was pursued vigorously, with the hope of finding the ultimate answers to all solar cell measurement problems. Yet spacecraft experiments cast doubt on the solar

data constant then being used, which had been the "spectral standard" for simulator performance.

During the mid-1960's significant progress was made in simulating solar energy in the laboratory. Most of this equipment was not simply directed toward solar cell testing but was also used widely for materials testing, determination of solar absorptivities and thermal balance testing on the subsystems and complete satellite systems. The solar simulators developed used high power, high pressure xenon arc lamps which operated continuously and illuminated reasonably uniformly an area up to nearly 0.07 m^2 with a closely matched (when appropriately filtered) air-mass-zero spectrum. A need for illuminating much larger areas and entire arrays, however, continued to exist until the so-called pulsed xenon arc solar simulators became available in the late 1960's. The pulsed solar simulators permit energy densities to be reached in the lamps which can be maintained only for a few milliseconds to prevent lamp destruction. These simulators can thereby provide illumination over an area of 5 meters in diameter at one solar constant intensity.

B. SINGLE CELL MEASUREMENTS

Silicon solar cells are semiconductor devices which convert light energy into electrical energy. Intensity and spectral distribution of the incident light energy, size of illuminated active cell area, and cell temperature are the main factors which determine the electrical output of a solar

cell. The cells are tested for their ability to convert a given amount of light energy into a specified amount of electrical energy.

A typical test setup consists of a light source which allows the beam of maximum intensity to be directed toward the solar cell. The cell is placed at a distance from the lamp with its active surface at a right angle to the optical axis of the light beam. Generally, the greater the distance, the more accurate the measurement. The operating voltage of the lamp is adjusted until its spectral distribution corresponds to a specified value and the intensity is adjusted by varying the distance between the lamp and solar cell.

C. PRESENT METHODS OF TESTING PHOTOVOLTAIC DEVICES

There are three general methods used to obtain I-V curves of solar cells, these methods are described in detail in Ref. 9. The three methods are named as follows:

(1) Photovoltaic Curve

(2) Diode Curve

(3) N-P Junction Characteristics

In method (1) the solar cell is illuminated and a variable resistance is used as the circuits load. As the resistance is varied from 0 to , the corresponding sets of output current and voltages are plotted as points on an I-V curve. For an automated system a programmable resistor would be used. This will increase the series resistance of the

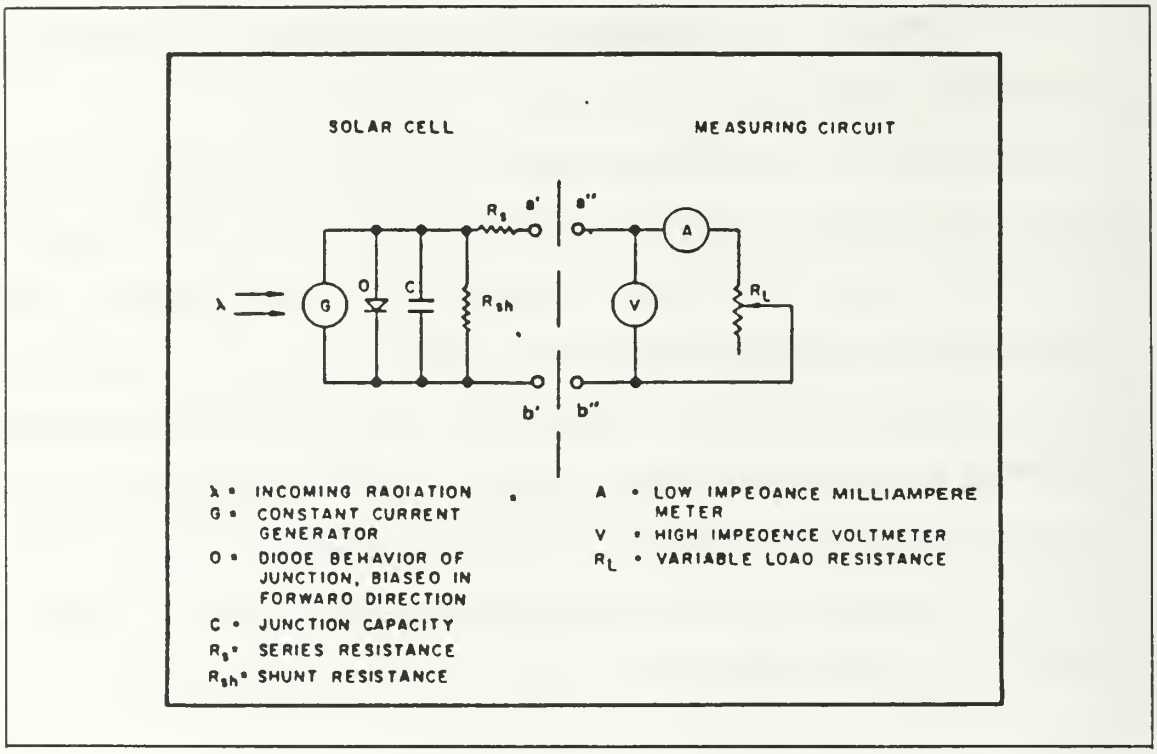

Figure 3.1 Measuring Circuit for Method 1.

cell due to the internal resistance of the CMOS switches which will produce ambiguous I-V curves (Figure 3.1).

In method (2) the solar cell is not illuminated. An external voltage is applied to the cell to forward bias the cell. The cell's voltage is varied thus causing the cell to act like a current sink. The corresponding values of voltages are matched with the resulting current values to generate data for an I-V curve.

In method (3) a source whose spectral output can be varied from zero to two AM0 (Air-Mass-Zero; sunlight concentration at Earth's orbit) is used. The step wise variation

of the source will create sets of I_{SC} and V_{OC} data points which can be used to create I-V curves.

Almost all I-V curves that are represented in publications are generated via method (1). The nonilluminated method (2), is used in conjunction with shadowing and array research. Method (3) is used mainly by solar cell manufactures in there research to build more efficient cells. The corresponding I-V curves generated by using the above three methods can be represented by the following equations. [Ref. 9]

$$I = I_L - I_o\{\exp[q/(AkT) * (V + IR_S)] - 1\}, \quad (3.1)$$

Method 1.

$$I = I_o\{\exp[q/(AkT) * (V - IR_S)] - 1\}, \quad (3.2)$$

Method 2.

$$I_{SC} = I_o\{\exp[q/(AkT) * V_{OC}] - 1\}, \quad (3.3)$$

Method 3.

The above methods have been used for many years and if used properly can generate very good I-V curves. The major disadvantages of these methods are the massive equipments needed to obtain the I-V data and their excessive power requirements. These drawbacks make these methods impractical

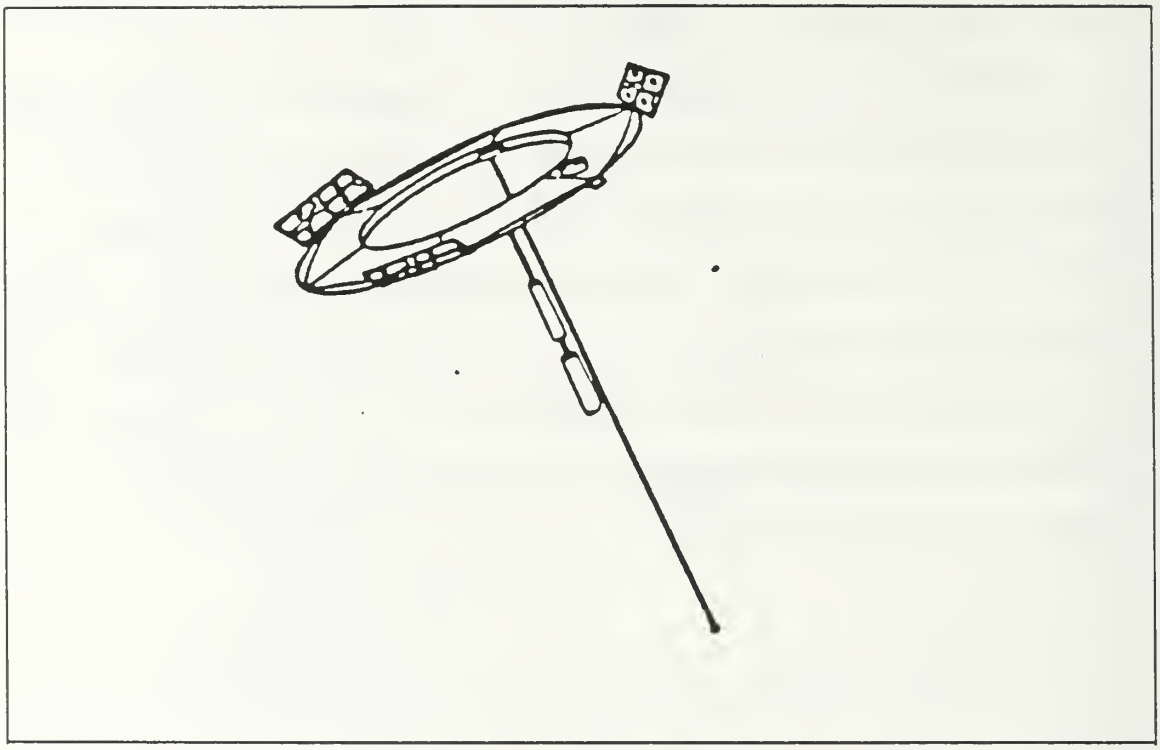

Figure 3.2 LIPS-II, Living Plume Shield

in a remote measuring system with all the environmental restrictions.

D. METHODS OF TESTING CELLS IN SPACE

1. LIPS-II Solar Cell Experiment

LIPS-II (Living Plume Shield) was launched by the Naval Research Laboratory (NRL) on 10 February 1983. This package was developed to test solar cell array panels in a low earth orbit (600 nm.) [Ref. 10]. The experiment consisted of three double-sided panels of solar cells (five panels were Si, one GaAs) these panels also powered to the satellite (Figure 3.2). [Ref. 12]

The primary significance of this experiment was that the panels were tested for the degradation of the panels versus testing each separate cell. Thus when the GaAs panel was tested all 300 cells were tested as an unit.

The test consisted of cycling each panel through V_{oc} to I_{sc}, via a loaded circuit (similar to method 1). Only seven points were obtained, with only four of these being in the proximity of "the knee" or maximum power point, P_{mp} (Figure 2.14).

The LIPS panel was designed as an add-on or "piggy-back" experiment, therefore the satellite did not behave as a normal satellite would. The satellite was free to yaw and its position with respect to the sun could not be controlled. The experimental package onboard was only controlled when the satellite was over the ground station.

These two idiosyncrasies caused significant gaps in the collection of data. One such gap occurred during the first thirty days of operation. The first data from the satellite showed a 6.9% (Figure 3.3) loss of power from the prelaunch statistics. This is such a significant loss that it was felt that the radiation models alone could not account for the decay. Mechanical failures internal to the array seems to be the most promising culprit. Some of these failures may have been contact or coverglass damage. [Ref. 10]

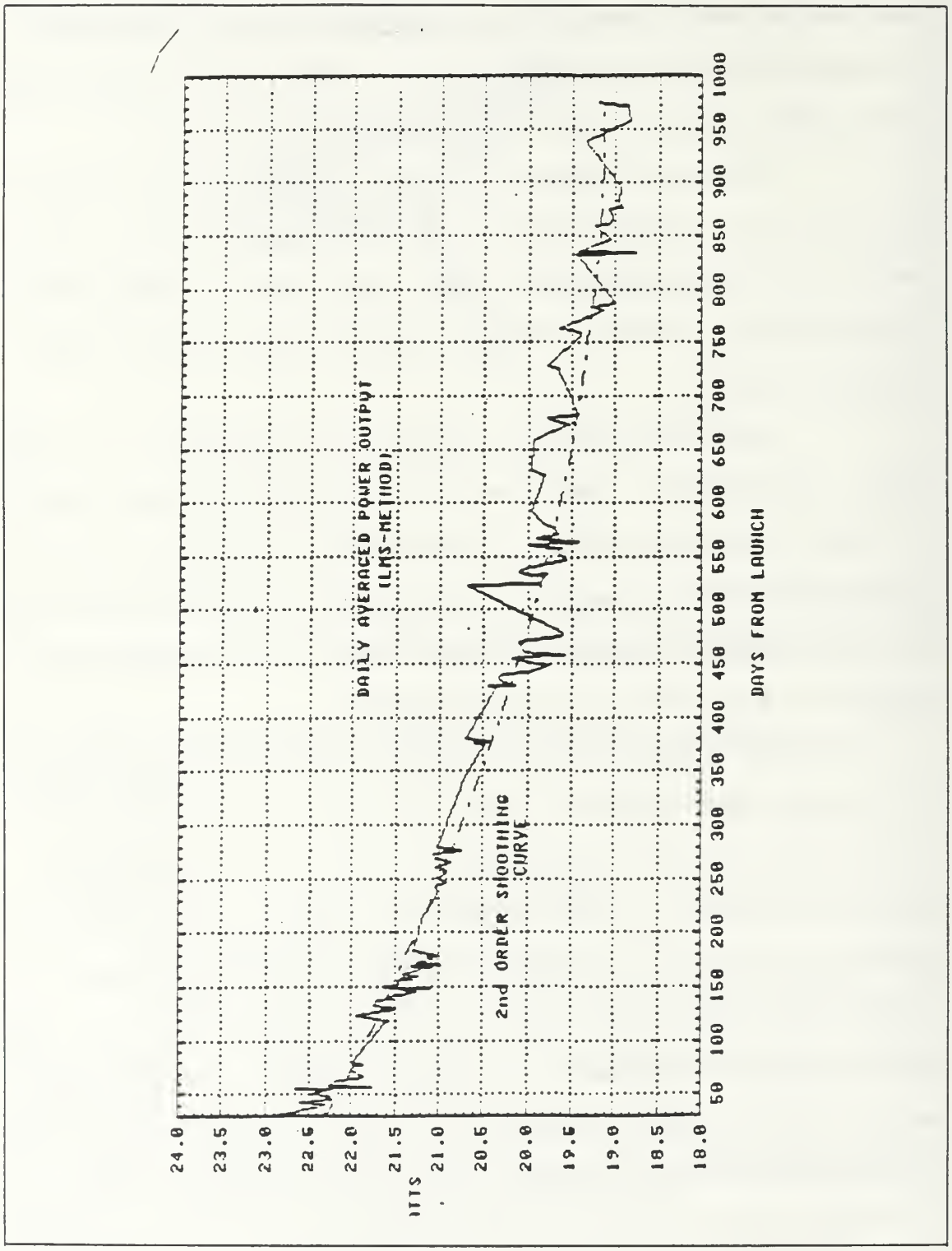

Figure 3.3 LIPS Maximum Power vs Days from Launch

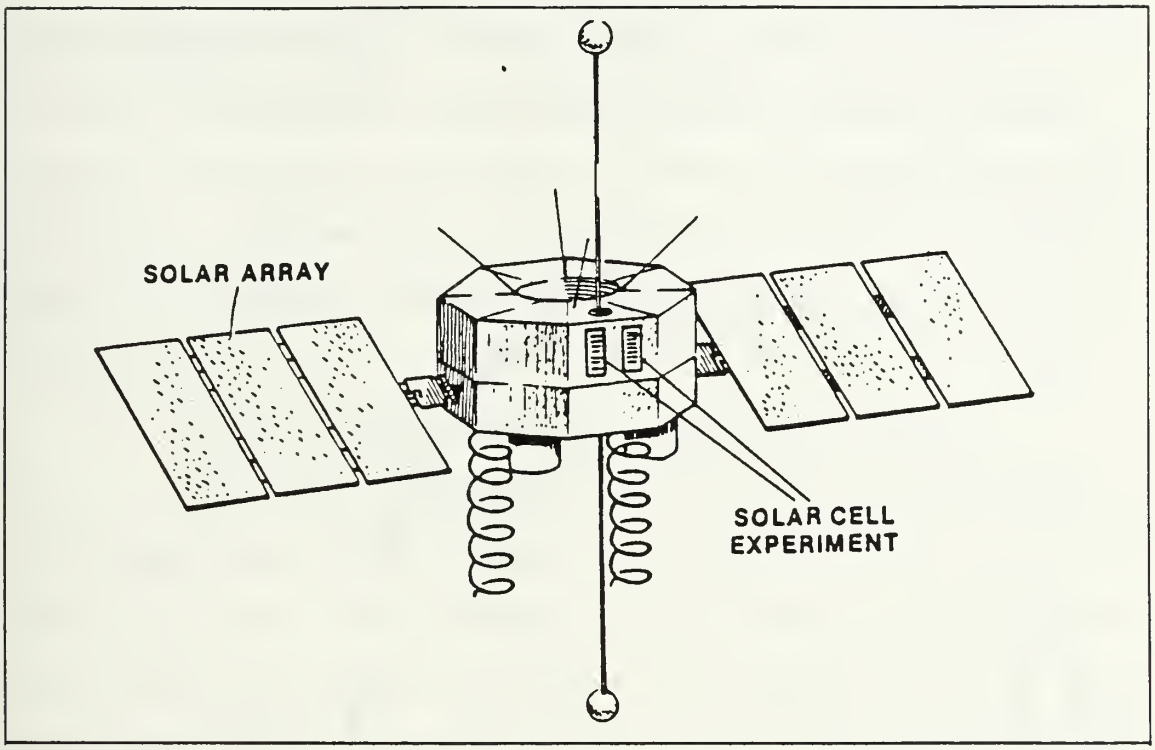

Figure 3.4 NTS-2 Satellite

2. NTS-2 Satellite

The Navigation Technology Satellite-Two is the second satellite in the series of development satellites that are the forerunners of the Global Positioning System (GPS) satellites that will be launched in the 1990's (Figure 3.4).

NRL was able to "piggy-back" a solar cell experiment on the NTS-2 satellite. This experiment was designed to help measure the degradation rates of selected cells as well as to determine the radiation resistance of state-of-the-art solar cells. The package consisted of 15 separate experiments each containing a five cell array. An I-V curve was generated by using a method similar to method (1) mentioned previously (Figure 3.5).

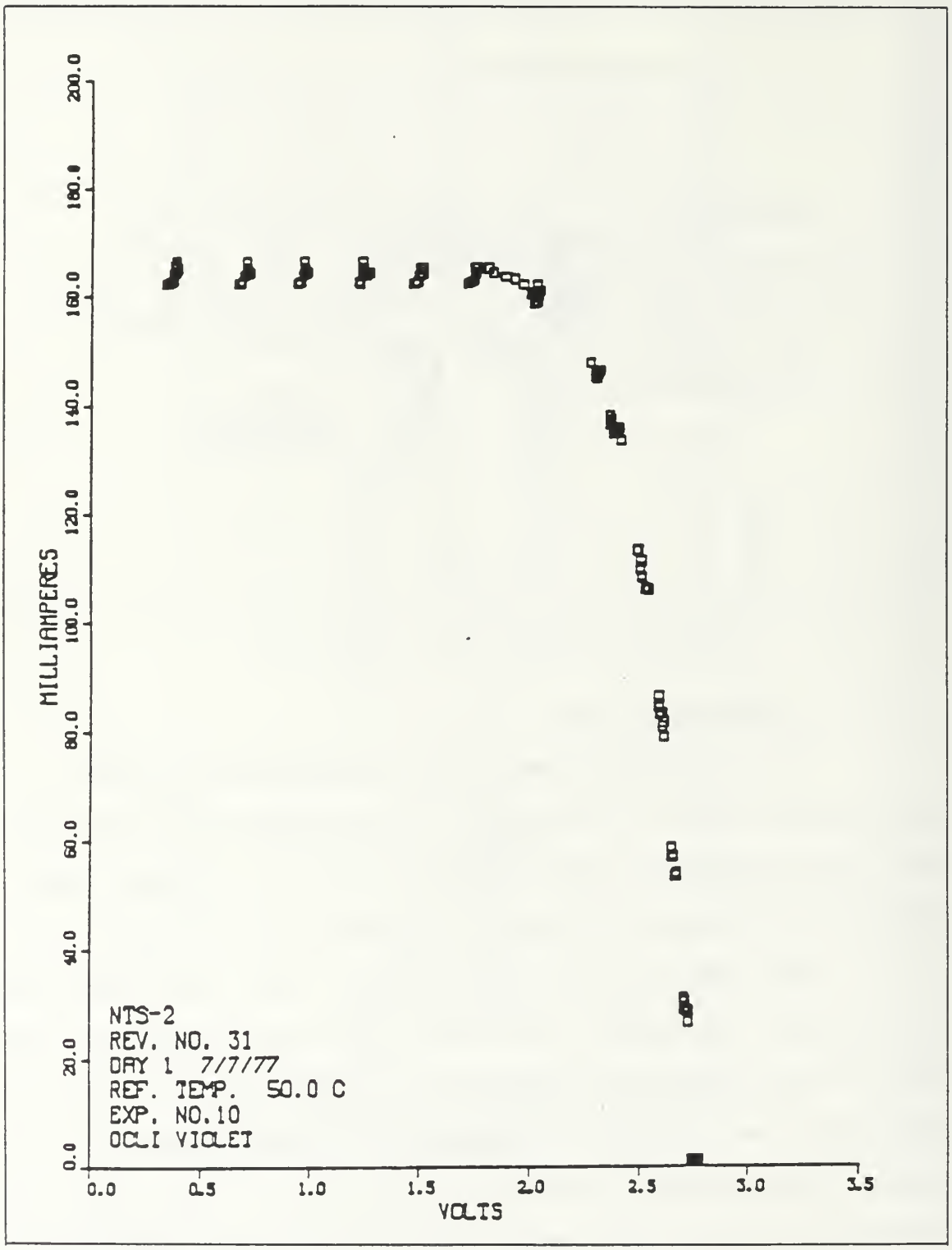

Figure 3.5 Typical NTS-2 I-V Curve

The GaAs cell aboard NTS-2 showed the biggest initial decrease, 12.3%. Though this difference was not entirely attributed to measurement error, because some annealing occurred, some change in the cell module obviously occurred. Whether this was a physical change in the solar cell or a change in the measuring circuit, has yet to be determined. [Ref. 12]

3. Solar Cell Calibration Experiment (SCCE)

The SCCE is designed to be flown on free flying platforms that are delivered into low earth orbit by the Space Shuttle. The SCCE major objectives are to generate calibrated solar cells for uses as standards in solar cell simulators and to compare accuracy and costs of space calibration with respect to ground testing. [Ref. 13]

The SCCE can measure two electrical parameters of up to a maximum of 32 solar cells. The parameters measured are V_{OC} and I_{SC}. Because of budget considerations a design to record the entire I-V curves was not included. The inability to record the temperature (or the entire I-V curve) will cause the data to be inaccurate. Though flown on two shuttle flights no significant calibration of solar cells on the SCCE has occurred.

E. SOLAR SIMULATOR AT NPS

The solar lab at NPS can be used to gather data from solar cells in near AM0 (sunlight at one astronomical unit from the sun) conditions. The solar cell testing facility

uses a procedure similar to method (1) to obtain solar cell I-V curves. Developed in 1985, the facility consists of five main components [Ref. 14]:

(1) Computer
The computer that is used to control the system is a IBM PC/XT. The test software is resident in the computers 20 megabyte hard disk. An Hewlett Packard 7475A plotter is used to plot solar cell I-V data.

(2) Data Acquisition and Control Element
A 12 bit, 4 channel analog-to-digital converter, internal to the IBM PC/XT is the major component of the Data Acquisition and Control Element. A digital multimeter is also included to provide current and voltage measurements. Both devices are controlled by the IBM PC/XT.

(3) Power Supply
The third component of the solar cell test facility is a programmable power supply, provided to operate as a current sink, allows for remote manipulation via the IBM PC/XT.

(4) Solar Simulator
A Kratos Solar Simulator makes up the fourth component of the solar lab. The solar simulator uses a Xenon arc lamp to generate an 12 inch circle of AM0 light (99% accurate [Ref. 14]). The lamp can deliver from 1000 to 7000 watts of power.

(5) Test block and Temperature Control
The test block uses a four point electrical connection to minimize the series resistance of the test circuit. A water circulation system, that is routed through the test block, is used to maintain the temperature of the solar cell at its desired level. The temperature can be maintained to within $\pm$ 0.5 degrees Celsius, over a range -20 to +70 degrees Celsius.

A more complete understanding of the solar cell lab maybe found in Gold [Ref. 14].

IV. NOVEL PHOTOVOLTAIC TESTING SYSTEM

A. PROPOSED CIRCUIT

As outlined in Chapter 3 there are a wide variety of methods to be used in obtaining solar cell data. Some of the earlier experiments for the evaluation of solar cell performances were conducted on single cells. The I-V curves generated in these experiments were interpolated from few fixed points concentrated around some predetermined P_{mp} points (Figure 2.14). During severe degradation these points do not always correspond to the actual P_{mp} point, since this point will change in degraded cells.

Other experiments tested strings of cells versus a single cell. This data has then been used to interpret the degradation of each cell in the array. While this procedure is valid it does not tolerate any failure of cell contacts, etc. A malfunction of a contact on the LIPS panel and on the NTS-2 satellite may have caused the unexplained initial power loss [Ref. 10]. Because of this problems and other types of failures it is felt that tests should be conducted on individual solar cells versus arrays. This will insure that one bad cell in an array will not cause false data for the remaining cells. If individual cell parameters are accurately measured then this data can be used to simulate array behavior in space.

Systems such as the solar cell testing facility at NPS can be considered state-of-the-art. The major drawbacks, as previously mentioned, are their rather large initial outlay of capital and the fact that they are quite bulky.

1. Design Requirements

From the above discussion a need for a low power, lightweight system (that is capable of accurately obtaining complete I-V curves of solar cells) is essential. These requirements are paramount when developing a system for the acquisition of data in a space environment. Such an autonomous system not only must survive the launch forces but it must operate for extended periods of time on very little power. This system can also be modified so that it could be a low cost alternative to a solar cell test facilities.

The following are a set of requirements needed for proper operation of the proposed system.

(1) Minimizing series resistance using current sinks.

(2) Circuit should have the ability to record data accurately.

(3) Circuit should have the capability to sink enough current to sweep from V_{OC} (open circuit voltage) to I_{SC} (short circuit current) points.

(4) Capable of measuring a series of multiplexed cells and sensors accurately.

(5) The internal resistance of the multiplexer CMOS switches should not affect the measured data.

(6) Circuit must be simple so components would occupy very little space.

(7) Thermal considerations of spacecraft require low thermal output from circuit.

(8) Require buffering of input and output signals to insure accuracy.

2. Alternative Circuits Considered

Early development of the circuit involved a setup where a capacitor was being charged using the test cell as a power source. The capacitor acts like a variable load. The current and voltage data of the cell can be measured while the capacitor is being charged. Current measurements require a resistance to be connected between the capacitor and the solar cell. The voltage across this resistance is linearly proportional to the cell current. While the cell terminal voltage would provide the data need for the I-V characteristics. The circuit was implemented and three major drawbacks were observed:

(1) The external resistance introduced in the circuit, increased the series resistance of the test cell thus degraded I-V characteristics were obtained (Figure 2.13).

(2) Since the capacitor charges exponentially, the data points obtained were not linearly distributed. This causes compression of the data at critical points on the knee of the curve.

(3) To get a practical time constant, a large capacitor was needed. The circuit developed would require a capacitor to be placed in each circuit. A system that would test many solar cells would be unmanageable due to the extreme weight and size of the capacitors.

A programmable resistor system was also investigated. This design was considered attractive due to its simplicity and low mass advantage. Discussion with engineers at NRL and Wright Patterson AFB revealed that this design was considered for deployment on a future Air Force satellite (CRESS-1). In this design the obvious added series resistance in the

circuit would cause false and degraded I-V characteristics as discussed in the previous method. Therefore this concept was considered inappropriate and other alternatives should be explored.

The use of a programmable power source was proposed. Though promising for terrestrial use, the size of the power source and its related components ruled out its use as a space based system.

B. NOVEL CIRCUIT DESIGN

A novel circuit was developed using a Bipolar Junction Transistor (BJT) in a Common Emitter configuration (Figure 4.1). The solar cell is used as the collectors load. By ensuring that the BJT has a high h_{fe} (eg. 2n3405; $h_{fe} > 400$; $I_C = 0.9975\ I_E$) this will allow the base current to be neglected with respect to the emitter current. Such that I_C approximates I_E; ie. solar cell current is directly proportional to the voltage across the resistor, R_E as shown in Figure 4.1.

A 10 volt source is used to forward bias the solar cell, this will allow sufficient current to flow through the resistor (Maximum I_{RE} = Isc). Cell current (I) is proportional to the voltage measured across the resistor, R_E. While the cell voltage (V) can be measured directly across the cell.

By sweeping the base current the transistor will go from the cutoff to saturation modes. This will drive the cell

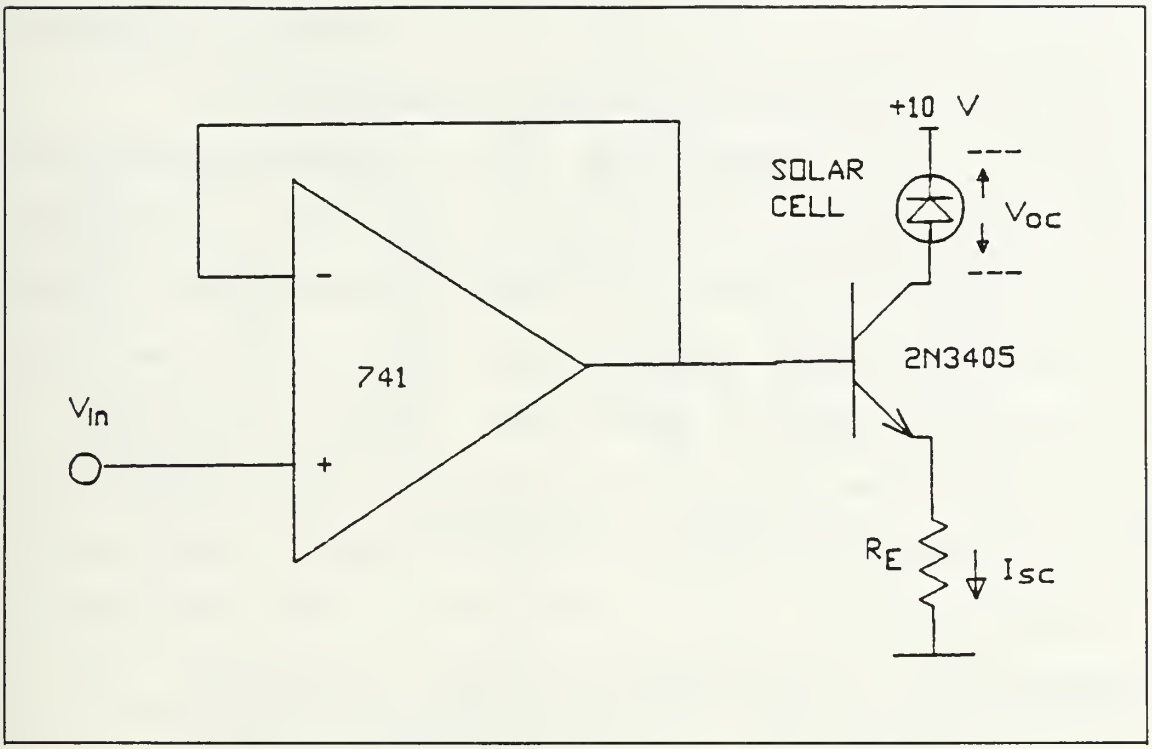

Figure 4.1 Novel Circuit Design

from V_{OC} to I_{SC} and produce the cell I-V curve. A selective ramp output from a Digital to Analog Converter (DAC) will be used to drive the base of the transistor.

1. Circuit Development

The development of a subcircuit was essential in the evolution of this research. The subcircuit shown in Figure 4.2 was (developed in the NPS production lab) etched onto a PC-board. This provided space for the semipermanent attachment to the PC-board of a solar cell. This process allowed the subcircuit to be tested with different types of transistors and operational amplifiers without fear of damaging the solar cell.

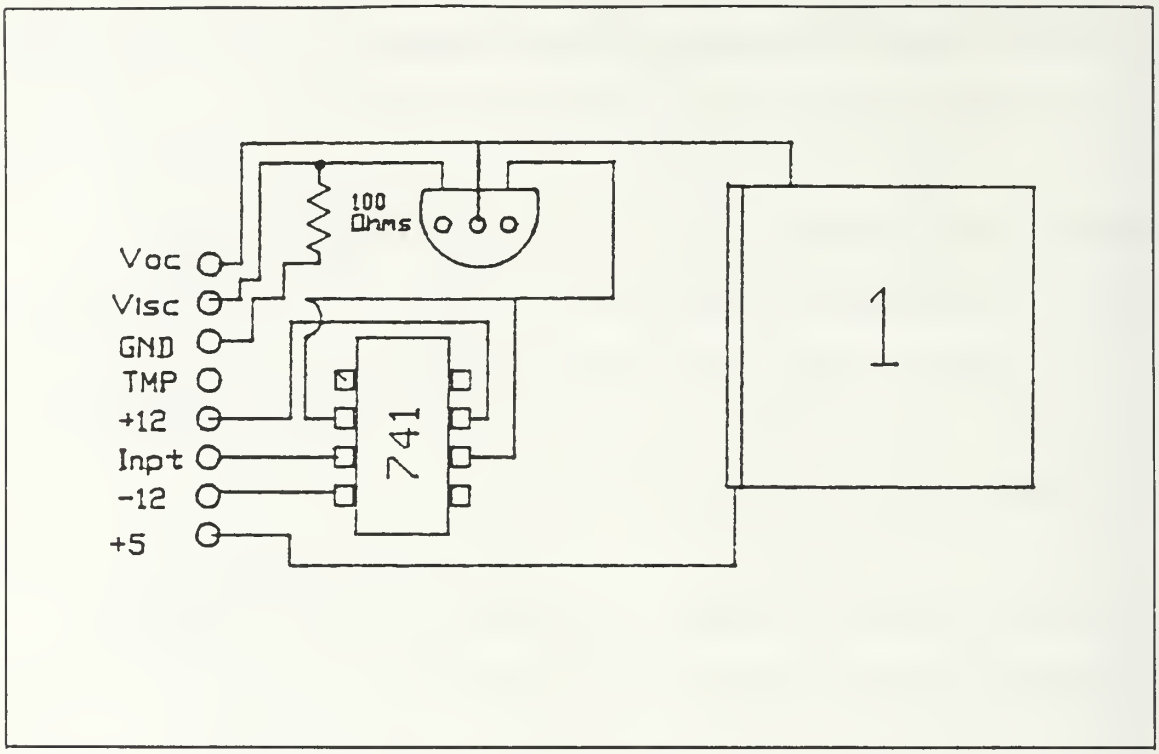

Figure 4.2 Solar Cell Subcircuit

Testing of the circuit was carried out using a DAC 0800 integrated circuit in series with an operational amplifier to provide an analog ramp voltage. This voltage was demultiplexed using a MUX 507 and then was directed to one of four subcircuits. The use of the operational amplifiers insured that the demultiplexer's internal resistance was prevented from altering the data received from the subcircuits.

Each subcircuit had three output data lines, two were for V_{OC} and I_{SC}. The third will be used for temperature data. Output data obtained from the subcircuits was buffered

by using operational amplifiers thus insuring the multiplexor internal resistance will not alter the accuracy of the data.

A counter circuit was developed to test the capabilities of the circuit as well as to simulate a microprocessor controller. The binary counter was incremented by the output clock of the function generator. The DAC 0800 digital input was then driven by the binary counter output, thus generating a linear ramp voltage. The current in each of the subcircuit's solar cell was swept from 0 to I_{SC} using the multiplexed ramp voltage of the DAC. Experimental results of this circuit are shown and discussed in the following chapter.

2. Controlling the Test Circuit using a Microprocessor

Using a microprocessor as a system controller provided an added advantage over the previous setup because it allows the circuit to operate as a fully integrated autonomous system. Such a system would have the following advantages:

(1) The ability to have preassigned data points would allow the experimenter to record data from the area of the I-V curve which is deemed important.

(2) Allow for different types of solar cells to be tested without major changes to the system.

(3) Diagnostics internal to the system would allow testing of it's program as well as it's circuit components.

(4) Would allow future experiments such as current annealing and concentrator tests to be added with very little change to the system.

The development of a low power, CMOS microprocessor controller by the Naval Postgraduate School (NPS) Space Group allowed the integration of the proposed circuit with a controller previously developed for the NPS Space Shuttle Bay Acoustic GAS project [Ref. 5]. This controller has the ability to store data in the INTEL 4 megabit Magnetic Bubble Memory (BPK 5V75).

The heart of the system is the NSC 800 microprocessor. The NSC 800 is mated with two NSC 810 I/O ports and is supported with 56 kilobytes of EPROM and 8 kilobytes of RAM. The ROM is used to store the series of subroutines that control the solar cell test circuit and format the data for transmission. The RAM will be used as a buffer for temporary storage of all the data until one cycle of the test is complete. The buffer will also allow the formatting of the data efficiently before storage in the bubble memory unit. This will conserve power since the bubble memory requires significant amount of power on initialization. The bubble memory unit allows a large amount of data to be stored until downlink, this will occur when the satellite is in view of the ground station.

The microprocessor drives an 8-bit DAC whose output is multiplexed to each individual solar cell test circuits through an analog multiplexor. The measured voltages (across each cell and across R_E) are buffered, multiplexed and converted to digital data using an ADC-0817 (Figure 1.1). The

resulting 8-bit words are stored in RAM until the conclusion of the test cycle.

The system was breadboarded using components similar to that of the controller being developed by the NPS Space Group for the Space Shuttle Bay Acoustic GAS Project. The system layout shown (Figure 4.3) was developed using the Z-80/Prolog system. The use of the Prolog system provided similarity to the envisioned final product. This verified the basic design and allowed the research to proceed.

Finally, the power supply requirements for each of the circuit components were taken into consideration. A single voltage source of 10 volts was used to resemble a typical satellite power supply. With the help of a solid-state voltage regulator, this single voltage was the soul source of power throughout the circuit.

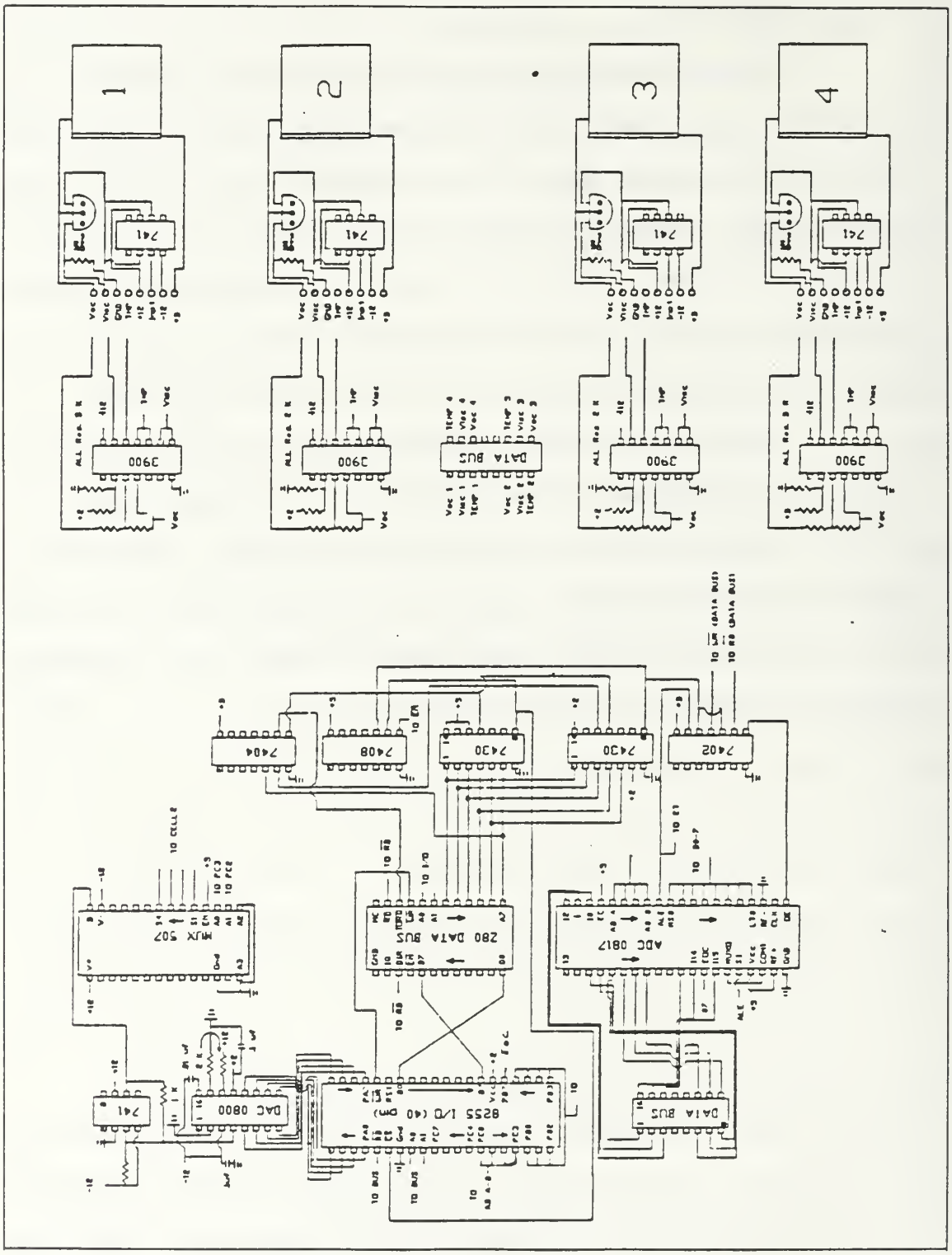

Figure 4.3 System Layout

V. CONCLUSIONS

A. RESULTS

Figures 5.1a, 5.1b, and 5.2 show the I-V characteristics plotted from the solar cell current and voltage data [Ref. 15]. The data was measured using the proposed novel design as well as a state-of-the-art measuring technique that requires the use of several sophisticated equipments controlled by an IBM PC/XT computer (using method 1). The curves of both figures (Figure 5.1 for silicon solar cells and Figure 5.2 representing GaAs cells I-V characteristics), show clearly the superiority and improvements of the measuring technique using the new proposed design. This is obvious since the new I-V curves experience sharper knees that correspond to smaller resistance in series with each of the cells. Moreover due to the simplicity of the new design, the proposed circuit was considered an excellent candidate for an autonomous system for remote testing.

B. RECOMMENDATIONS

Several problems were encountered during this research. Two of these were of such significance that they inhibited the flow of the research.

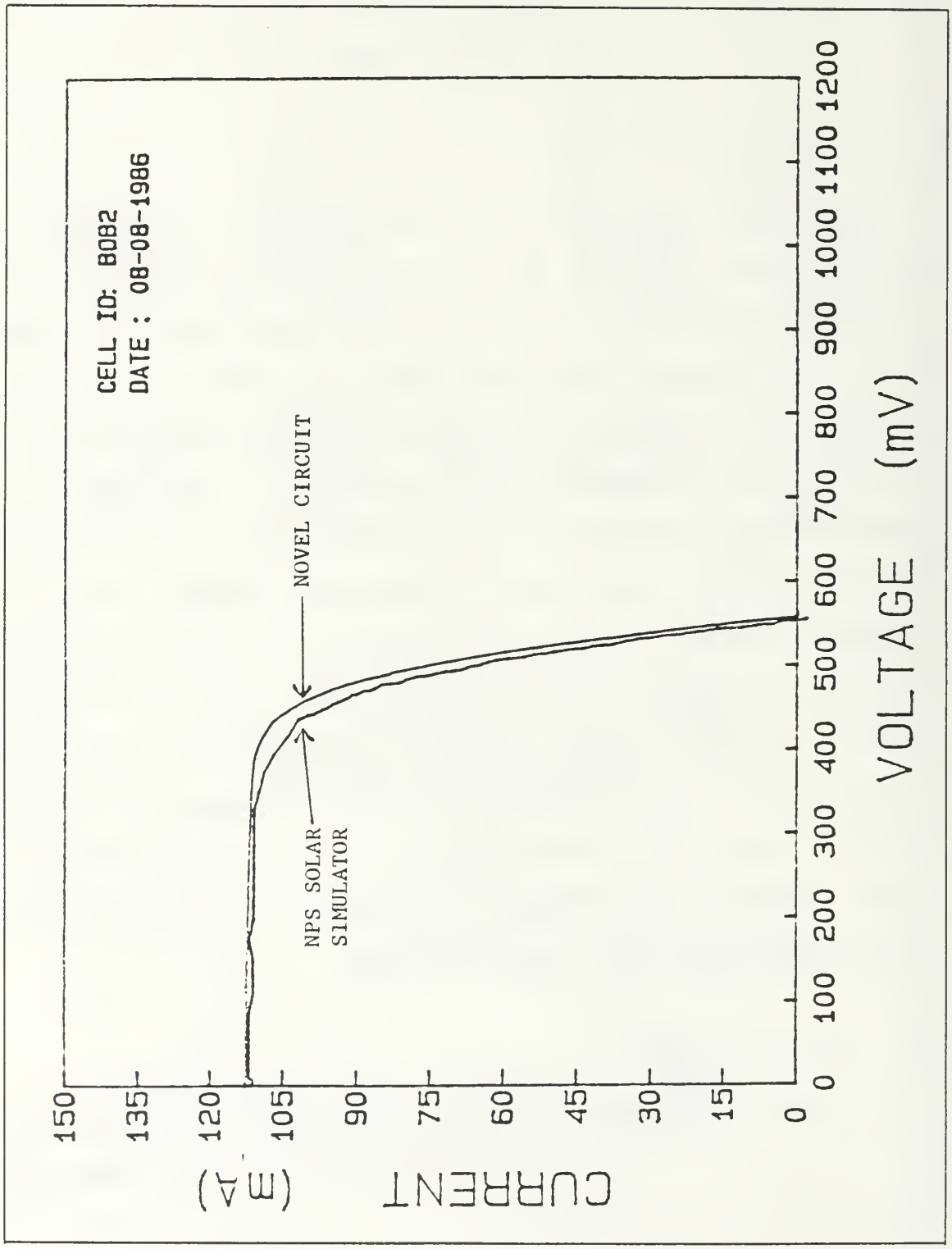

Figure 5.1a Comparison Data, Silicon

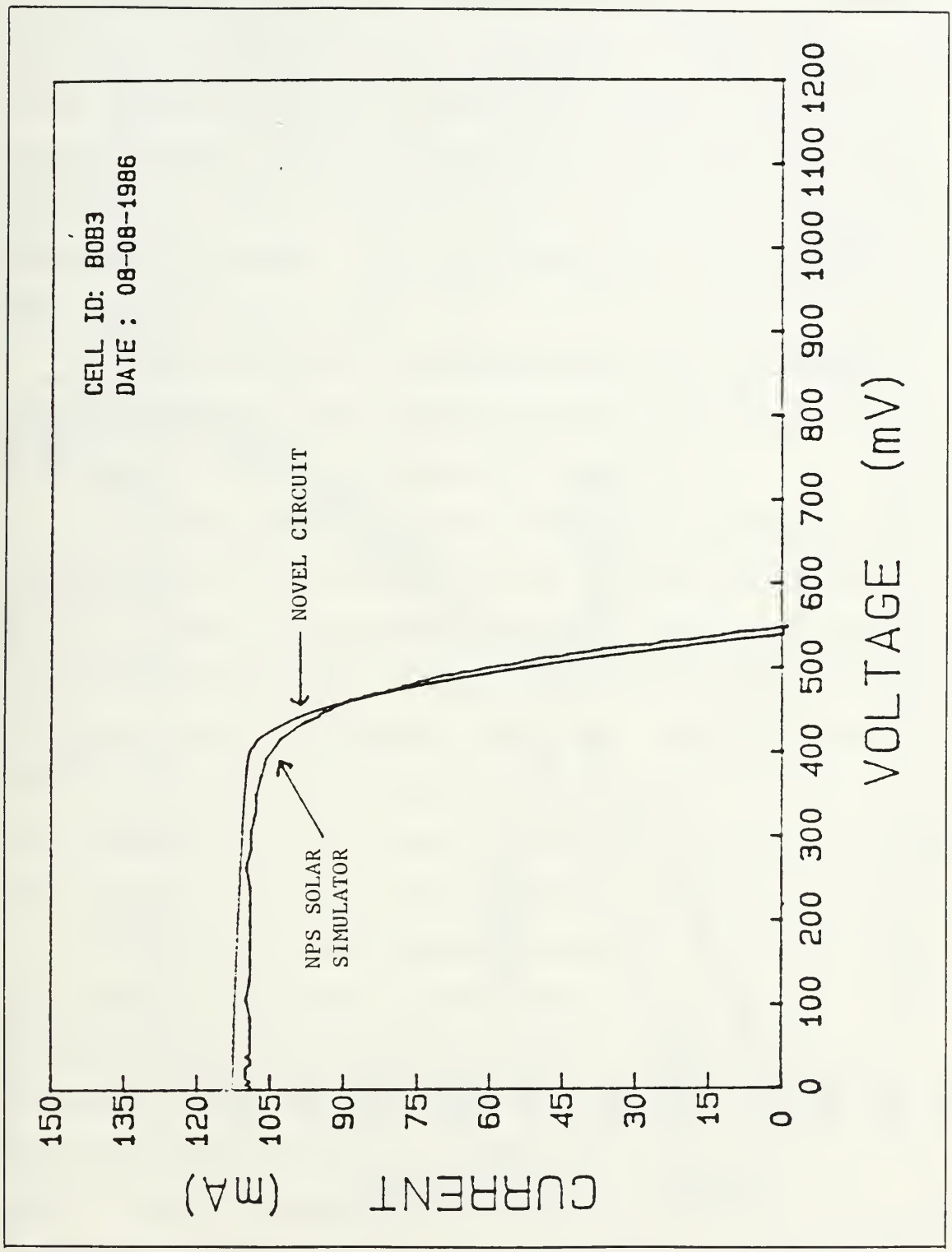

Figure 5.1b Comparison Data,Silicon

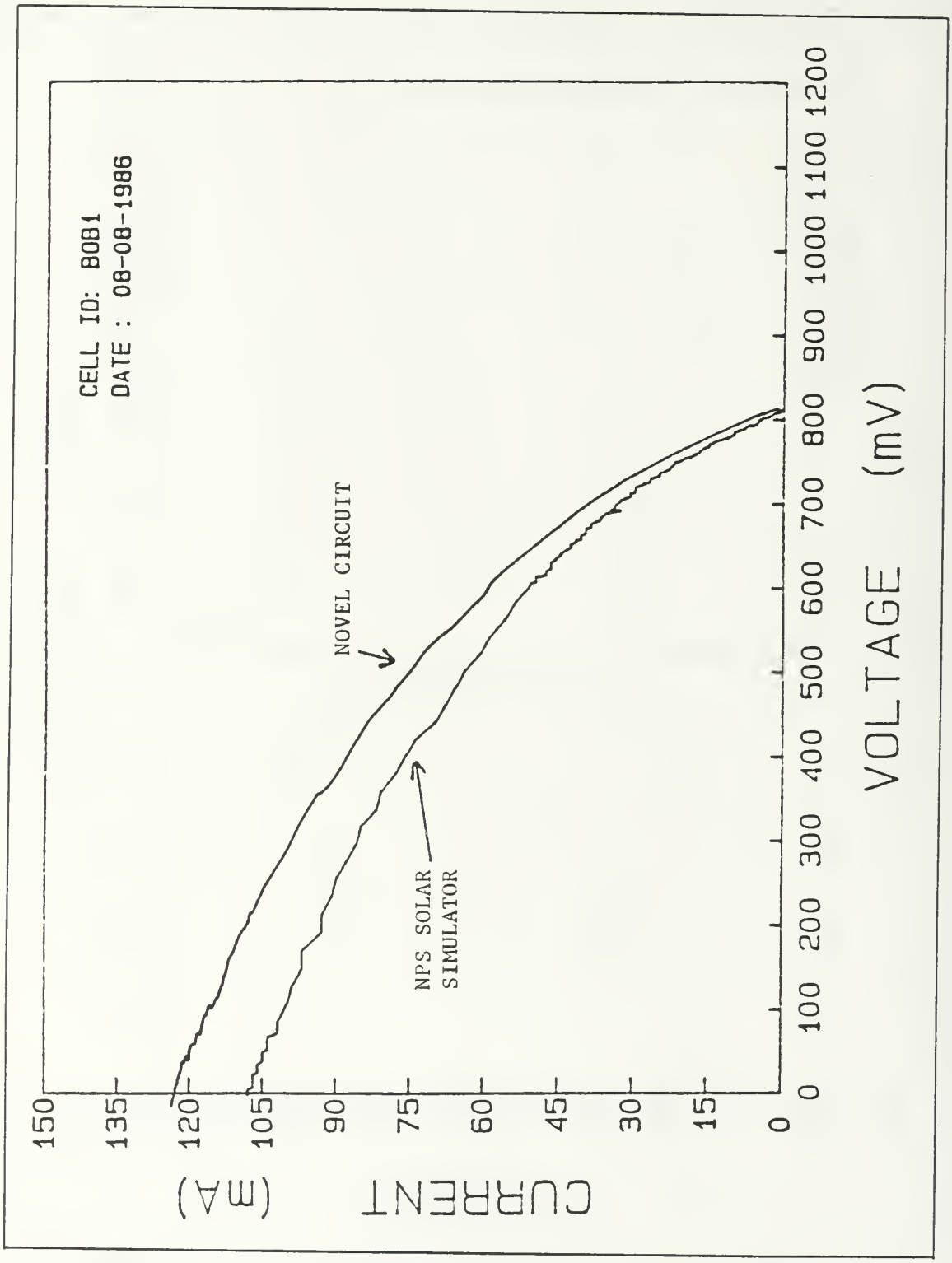

Figure 5.2 Comparison Data, Gallium Arsenide

The first problem encountered was the soldering of GaAs and Si solar cells to devices or arrays. These devices need to be welded instead of soldered into place. Soldering causes a higher series resistance that will degrade the performance of the cells and causes inaccurate characteristics to be recorded. This was referred to in Section D of Chapter II (Figure 2.13).

The acquisition of a welding device will solve this problem and improve the accuracy of the data when working with state-of-the-art photovoltaic devices.

The second problem was the inability to interface an analog device to a computer without designing an I/O port that is unique to a particular design. This causes wasted time constructing novel I/O ports when there are commercially available analog to digital interfaces. These interfaces will work with most IBM compatible computers. It is felt that purchase of one of these devices would greatly enhance the students ability to develop novel circuits and systems.

In conclusion, this research resulted in the development of a simple, low power, microprocessor based system. The proposed design would be very useful in remote testing of different solar cells and sensors to study the impact of the harsh space environment on state-of-the-art devices or for use in linear accelerators. The system could also be used in JPL's balloon testing program as is described in Ref. 6.

LIST OF REFERENCES

1. Wise, J. F., "Solar Power Requirements for Military Space Vehicles", Seventeenth IEEE Photovoltaic Specialists Proceedings,pp. 17-22, May 1984.

2. Loferski, J. J., "Photovoltaics 1: Solar Cell Arrays", IEEE Spectrum, pp. 26-31, February 1980.

3. Stivenard, D. and Bourgin, J. C., "Degradation and Recovery of GaAs Solar Cells Under Electron Irradiation", Seventeenth IEEE Photovoltaic Specialists Proceedings, pp. 1103-1108, May 1984.

4. Trumble, T. M. and F. Betz, "Evaluation of Gallium Arsenide Solar Panel on the LIPS II Satellite", Seventeenth IEEE Photovoltaic Specialists Proceedings, pp. 1108-1113, May 1984.

5. Boyd, A. W., Kosinski, B. P. and Weston, R. L., "Autonomous Measurements of Space Shuttle Payload Bay Acoustics During Launch", Submitted to Naval Research News, July 1986.

6. Jet Propulsion Laboratory, Publication 82-69, Solar Cell Radiation Handbook, California Institute of Technology, Pasaedena, California, 1982.

7. Jet Propulsion Laboratory, Publication 43-38, Solar Cell Array Design Handbook - Volume 1, California Institute of Technology, Pasaedena, California 1976.

8. Garlick, J., Course on Solar Cells, Part II, Class notes from Spectrolab, 1984.

9. Rauschenbach, H.S., Solar Array Design Handbook, Van-Nostrand Reinhold, New York, pp. 135-197, 1980.

10. Francis, R.W. and Betz, F.E., "Two Years of On-Orbit Gallium Arsenide Performance from the LIPS Solar Cell Panel Experiment", Proceeding of Space Photovoltaic Research and Technology Conference, pp. 1-12, May 1985.

11. Morris, R.K., "New Insight into the LIPS-II GaAs Solar Panel Performance", Proceedings of the Eighteenth Photovoltaic Specialists Conference, pp. 961-965, October, 1985.

12. Naval Research Laboratory, NRL Memorandum Report 3935, Results of the Solar Cell Experiments Aboard the NTS-2 Satellite after 447 Days in Orbit, by D. H. Walker and R. L. Statler, pp. 1-47, March, 1979.

13. Suppa, E.G., "Space Calibration of Solar Cells. Results of 2 Shuttle Flight Missions", Proceedings of the Seventeenth Photovoltaic Specialists Conference, May 84.

14. Gold, D.W., High Energy Electron Radiation Degradation of Gallium Arsenide Solar Cells, M.S. Thesis, Naval Postgraduate School, Monterey, California, pp. 25-29, March 1986.

15. Micheal, S. and Callaway, R., "A Microprocessor Based System for the Evaluation of Radiation Effects on Solar Cells in a Space Environment", to be published in the Proceedings of Twenty Ninth Midwest Symposium on Circuits and Systems, Lincoln Nebraska, August 1986.

INITIAL DISTRIBUTION LIST

		No. Copies
1.	Defense Technical Information Center Cameron Station Alexandria, VA 22304-6145	2
2.	Library, Code 0142 Naval Postgraduate School Monterey, CA 93943-5002	2
3.	Professor S. Michael Code 62Mi Naval Postgraduate School Monterey, CA 93943-5000	4
4.	Department of the Navy Commander Space and Naval Warfare Attn: Major M.L. McNulty Washington, D.C. 20363-5000	2
5.	Dr. H.B. Rigas Code 62 Naval Postgraduate School Monterey, CA 93943-5000	2
6.	Naval Space Command, Code N13 Dahlgren, VA 22448	2
7.	Fred Betz Code 6623 Naval Research Laboratory 4555 Overlook Ave., SW Washington, D.C. 20375	2
8.	Terry Trumble Energy Conversion Branch Aerospace Power Division Aero Propulsion Laboratory Wright-Patterson Air Force Base Ohio 45433	2
9.	Professor H. Titus Code 62Ts Naval Postgraduate School Monterey, CA 93943-5000	2
10.	Vice Commander United States Space Command Peterson AFB, CO 80914-5001	1

11. FL2058 Space Libary 1
HQ AFSPACECOM/MPSL
Peterson AFB, CO 80914

12. R. Francis 2
The Aerospace Corporation
P.O. Box 92957
Los Angeles, CA 90009

13. LT. R.K. Callaway 5
Air Department
USS MIDWAY CV 41
FPO San Fransico, CA 96631-2710

220136

Thesis
C19145 Callaway
c.1 An autonomous circuit for measurement of photo-voltaic devices parame-ters.